Desert dust aerosol columnar properties over ocean and continental Africa from Lidar in-Space Technology Experiment (LITE) and Meteosat synergy

S. Berthier,[1,2] P. Chazette,[1] P. Couvert,[1,3] J. Pelon,[4] F. Dulac,[1] F. Thieuleux,[1] C. Moulin,[1] and T. Pain[5]

Received 16 December 2005; revised 12 July 2006; accepted 28 July 2006; published 2 November 2006.

[1] The new generation of spaceborne backscatter lidar systems, prefigured by the Lidar in-Space Technology Experiment (LITE) mission in September 1994, will give new insight on the vertical distribution of both aerosols and clouds in the atmosphere. This is especially of importance for aerosols over land, where retrievals from passive sensors are known to be more difficult because of the surface contribution. Here we analyze mineral dust aerosol transport events through a new approach coupling the active LITE and passive Meteosat-5 spaceborne observations. The Meteosat-derived aerosol optical thickness at 550 nm is shown to be a good boundary condition for the lidar inversion in order to retrieve both the aerosol backscatter to extinction ratio (BER) and the aerosol extinction vertical profile above the Tropical Atlantic Ocean (TAO) and the Mediterranean Sea. Sensitivity tests indicate that the aerosol scattering coefficient is retrieved within a 20% relative uncertainty. Air mass trajectories allow us to further retrieve the vertical profile of aerosol optical properties over the continent in the Saharan Heat Low (SHL) region using the BER determined over the ocean. Results confirm a large dispersion of the BER which is not attributed to errors in the method. This shows the need to account for such dispersion in the retrieval of dust aerosol optical thickness and aerosol impact on the earth radiative budget. The coupling between LITE and Meteosat-5 made here is shown to be interesting for an improvement of the direct dust aerosol forcing, and results should be improved by the CALIOP-MODIS synergy.

Citation: Berthier, S., P. Chazette, P. Couvert, J. Pelon, F. Dulac, F. Thieuleux, C. Moulin, and T. Pain (2006), Desert dust aerosol columnar properties over ocean and continental Africa from Lidar in-Space Technology Experiment (LITE) and Meteosat synergy, *J. Geophys. Res.*, *111*, D21202, doi:10.1029/2005JD006999.

1. Introduction

[2] Tropospheric aerosol particles play a major role on the atmospheric processes involved in the radiative balance [e.g., *Léon et al.*, 2002], the photochemistry [*Boucher*, 1995; *Dickerson et al.*, 1997; *Randriamiarisoa et al.*, 2004] and the cloud formation [*Andreae*, 1996; *Seinfeld and Pandis*, 1998; *Rosenfeld*, 2000; *Charlson et al.*, 1992, 1999]. Because of their spectral characteristics and their high optical depth, mineral dust has been shown to have a very important direct radiative impact [*Fouquart et al.*, 1986; *Quijano et al.*, 2000; *Ackerman and Chung*, 1992; *Cautenet et al.*, 1992; *Haywood et al.*, 2003]. Dust can be suspected to induce a significant dynamical perturbation of the synoptic flow close to desert regions such as North Africa [*Alpert et al.*, 1998].

[3] The difficulty encountered to study the atmospheric aerosol, and especially the mineral dust aerosol, is due to the heterogeneity in both space and time of their concentrations and properties, due to the variety of their sources [e.g., *Prospero et al.*, 2002], their relatively short life time, and the complexity of their composition that evolve during their transport including possible interactions with clouds [e.g., *Chester*, 1986; *Guieu et al.*, 2002]. Furthermore satellite measurements, which are good approaches to characterize the occurrence of dust aerosols, are difficult to use for quantifying their impact over desert, because of the poorly known and high reflectance of the surface [*Chu et al.*, 2002].

[4] Numerous passive instruments on spaceborne platforms have been used to measure the column dust aerosol optical thickness over the ocean. Measurements were first derived from meteorological satellites Meteosat [e.g., *Dulac et al.*, 1992; *Jankoviak and Tanré*, 1992; *Moulin et al.*, 1997a, 1998] and AVHRR (Advanced Very High Resolution Radiometer) [e.g., *Stowe et al.*, 1992; *Husar et al.*,

[1]Laboratoire des Sciences du Climat et de l'Environnement, Gif-sur-Yvette, France.
[2]Also at Service d'Aéronomie du Centre National de la Recherche Scientifique, Université Paris VI, Paris, France.
[3]Deceased 6 June 2005.
[4]Service d'Aéronomie du Centre National de la Recherche Scientifique, Université Paris VI, Paris, France.
[5]Alcatel Space, Cannes, France.

0148-0227/06/2005JD006999

1997]. A new generation of passive instruments was developed in order to investigate the directional, and the spectral signature of aerosols. POLDER (POLarisation and Directionality of Earth Reflectance) is one of these instruments, which offers in addition polarized measurements [e.g., *Deschamps et al.*, 1994; *Deuzé et al.*, 1999]. More recently, *Tanré et al.* [1997] used multispectral informations extending from 0.55 μm up to 2.13 μm as provided by MODIS (Moderate-Resolution Imaging Spectroradiometer) to retrieve the aerosol properties and distinguish between fine and coarse aerosol contributions. Aerosol optical thickness (AOT) can also be obtained from MODIS over continental surfaces with low reflectance [*Kaufman et al.*, 1997], but only TOMS (Thematic Ozone Mapper Spectrometer) [*Herman et al.*, 1997; *Chiapello and Moulin*, 2002; *Ginoux and Torres*, 2003] and Meteosat infrared channels [*Legrand et al.*, 1992; *Hamonou et al.*, 1999] have yet provided valuable aerosol information over desert. The possibility of retrieving aerosol parameters in specific regions of the atmosphere is also provided by infrared sounders [*Pierangelo et al.*, 2004], but analysis over land is more difficult because of spatial variability of the surface emissivity.

[5] These passive instruments alone give only access to integrated information in the atmospheric column over the sea surface, and to sparse quantitative information above continents. The vertical distribution of aerosols in the atmosphere is, however, a key element of the Earth radiative budget [*Intergovernmental Panel on Climate Change*, 2001] that needs to be assessed at the global scale. The visible/near-infrared backscatter lidar is one of the most powerful and sensitive tool for the detection of atmospheric scattering layers above both continent and ocean with a high vertical resolution. Indeed, the Lidar in-Space Technology Experiment (LITE) on board the Space Shuttle in 1994 has clearly demonstrated the great potential of a spaceborne lidar for the determination of improved cloud and aerosol climatologies at global scale [e.g., *Winker et al.*, 1996; *Karyampudi et al.*, 1999] (http://www-lite.larc.nasa.gov/). This spaceborne mission has been recently followed by the Geoscience Laser Altimeter System (GLAS) mission [*Zwally et al.*, 2002] and will be relieved by the Cloud-Aerosol Lidar and Infrared Pathfinder Satellite Observations (CALIPSO) mission launched on April 2006 [*Winker et al.*, 2002].

[6] The difficulty in active remote sensing lies in the possibility of constraining the lidar signal inversion [e.g., *Klett*, 1981; *Sicard et al.*, 2002]. Combining range-resolved active measurements by lidar systems and column-integrated measurements by passive radiometers can lead to significant improvement of the lidar inversion and profiling capability and integrated measurement of radiometers [e.g., *Pelon et al.*, 2002; *Léon et al.*, 2002; *Chazette*, 2003; *Dulac and Chazette*, 2003; *Kaufman et al.*, 2003].

[7] *Chazette et al.* [2001] presented an analysis of a dust event observed in the Azores region combining Meteosat and airborne lidar data. With the forthcoming coincident active and passive aerosol observations of the spaceborne Aqua-Train mission in mind, we further present in this paper the potential of the coupling between a spaceborne lidar and a geostationary satellite to measure the aerosol optical properties over both ocean and continent, with a focus on African dust. We address the problem of the aerosol analysis over a high-reflectance surface as the Saharan desert. The passive and active observations selected are presented in the following section. In section 3 we describe the dust events observed with the help of Meteosat infrared observations, air mass trajectories, and a dust emission model. In section 4 the method we propose to benefit from the synergy between LITE and Meteosat 5 to retrieve the aerosol backscatter to extinction ratio (BER) is presented. The results in terms of the dust BER and aerosol optical thickness are shown in section 5 and discussed in section 6. The impact of the BER variability on the retrieval of the dust radiative budget over both ocean and continent is discussed in section 7.

2. Basic Spaceborne Observations

[8] The spaceborne observations to be coupled were performed in September 1994. They include data from the passive radiometer on board the European geostationary satellite Meteosat-5, and from the active lidar instrument on board the US space shuttle during the LITE mission.

2.1. Meteosat-5

[9] Meteosat-5 performed wide-band measurements in both the solar (VIS) and thermal infrared (IR) spectral domains. Images were obtained from EUMETSAT (Darmstadt, Germany). We have used full resolution (2.5×2.5 km^2 at nadir, i.e., $0.02^\circ \times 0.02^\circ$) VIS images taken daily at 1100, 1200 and 1300 UTC to retrieve the AOT over the ocean. We will describe our ancillary use of IR images later in section 3.

[10] The retrieval of the AOT at 550 nm for clear air pixels over the ocean surface is based on the look-up table algorithm defined by *Dulac et al.* [1992] and on the Meteosat-5 VIS sensor calibration of *Moulin and Schneider* [1999]. This algorithm has been validated by comparison of resulting AOTs to direct measurements by Sun photometers performed in the TAO and western Mediterranean [*Moulin et al.*, 1997b]. AOT results from 1100 to 1300 UTC have been averaged to improve the geographical coverage limitation by clouds. The map of dust AOT over ocean shown in Figure 1 is the average of daily maps obtained between 12 and 19 September. A significant dust plume over the TAO can be observed west of Mauritania ($\sim$20°N) with an 8-day mean AOT of 0.39 at 550 nm.

2.2. LITE

[11] The LITE experiment on board the Shuttle provided observations between 9 and 20 September 1994 which are available from NASA (http://www-lite.larc.nasa.gov). The lidar characteristics have been intensively described by *Couch et al.* [1991], *McCormick et al.* [1993] and *Winker et al.* [1996]. The LITE system was pointed toward the earth at an angle of about 5° to the nadir to minimize the possible specular reflection effects on clouds [e.g., *Platt et al.*, 1999]. Data used here are raw lidar signals at 532 nm obtained from several nighttime orbits that crossed northwestern Africa, the tropical Atlantic Ocean (TAO) and the Mediterranean. By visual examination of the quicklooks, we have selected exploitable observations with no saturation and with significant desert dust aerosol plumes. The selected orbital tracks, which were performed in the period 12–19 September, are

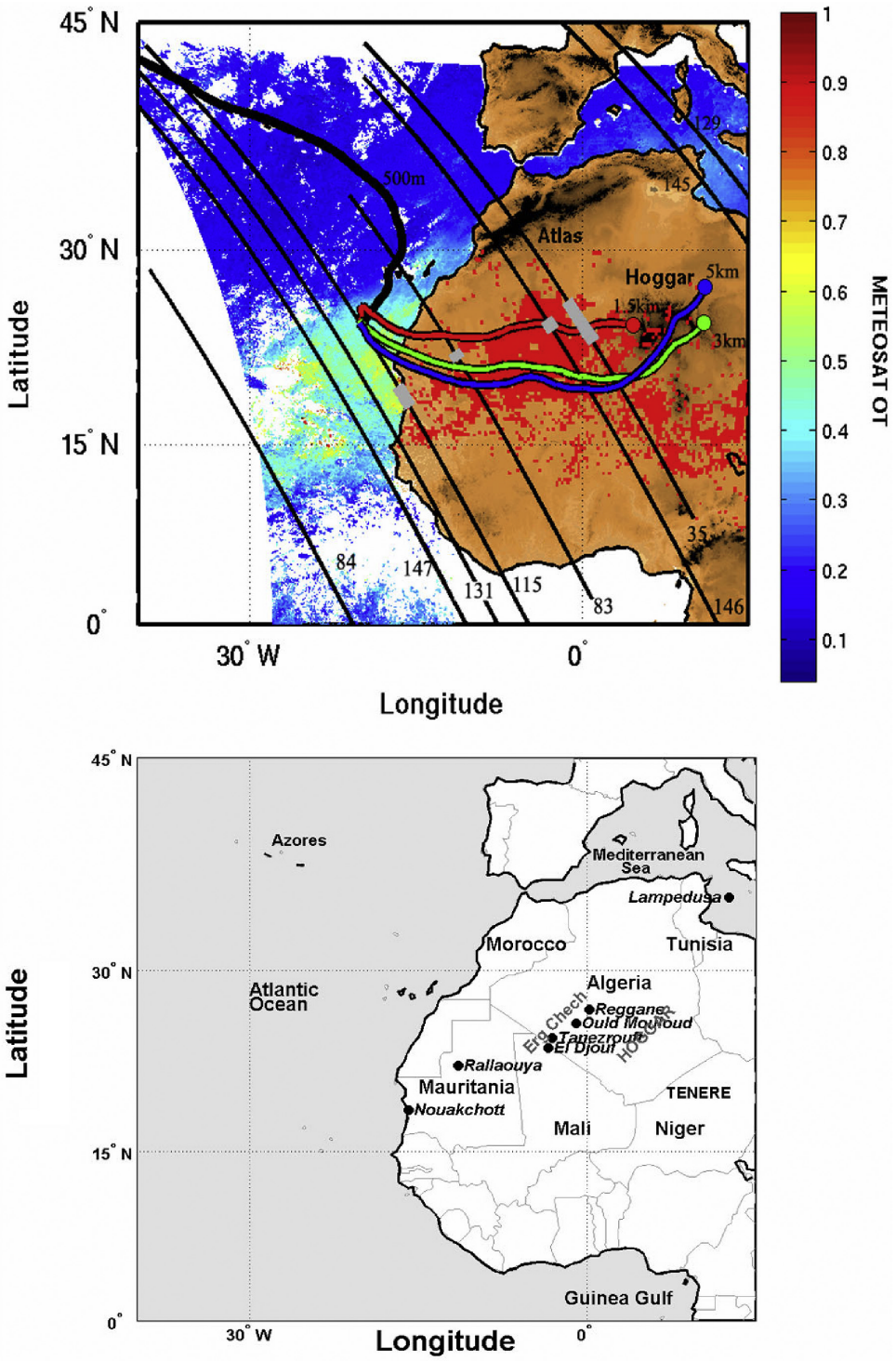

Figure 1. (top) Composite of dust optical thickness of dust over ocean (color scale), high-turbidity areas over Africa (red dots), and LITE orbital tracks for the period 12–19 September 1994. In addition, four 6-day back trajectories (courtesy of NOAA Air Resources Laboratory http://www.arl.noaa.gov) are plotted, ending on orbit 115 (17 September, 0100 GMT): the black back trajectory starts at 500 m amsl and ends at ~2.5 km amsl in the NW Atlantic; the red, green and blue back trajectories start at 1.5, 3 and 5 km amsl, respectively, and end at ~4.4, ~4 and ~4 km above Sahara, respectively. Gray sectors on the orbits give the location of the dust uptake as detected from LITE observations. (bottom) Main locations considered in this article.

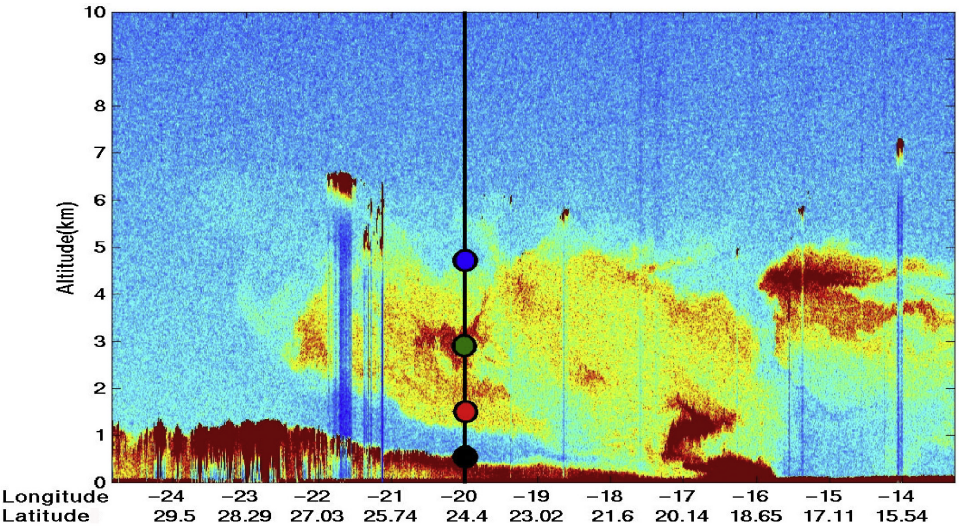

Figure 2. Raw LITE data of orbits 115 for 17 September 1994. The orbit crosses the northern Mauritanian coast at about 20°N. A dust uptake seems to occur between 18.5 and 20°N. The marine atmospheric boundary layer is very shallow close to the coast but reaches more than 1 km in the northwest of the dust plume area. Colored circles mark the starting points of back trajectories shown in Figure 1.

plotted in Figure 1. An example of the raw LITE data is given in Figure 2 for 17 September (orbit 115) over the TAO and western Africa. The dust layer extends up to more than 5 km in altitude. This section is particularly interesting because it shows both dust transport over the TAO up to about 23°W, and dust uptake from the western coast of Africa around 18.5°N and 16°E, where intense lidar signal is observed down to the desert surface. Three other regions of likely dust uptake have also been identified on orbits 35, 83 and 146 (12, 15 and 19 September, respectively) and their location is highlighted with gray shading on the orbits plotted in Figure 1. In Figure 2 the dust plume reaches the altitude of 4 km over the source area likely because of dry convection in the boundary layer. Ground-based lidar observations confirm dust at such altitude over Chinese desert areas [*Yasui et al.*, 2005] and *Takemi et al.*'s [2006] simulations of Chinese dust emissions indicate that both dry and moist convection play a role in the vertical export of dust to the free troposphere. Advection over the TAO may modify the vertical structure as particles are transported above the marine atmospheric boundary layer (MABL). It is interesting to note how the height of the MABL is regularly decreasing between 22°W and the coast at about 16.5°W, starting at 1 km in the remote TAO. At 20°W, the vertical structure includes from below (1) the MABL, (2) a free tropospheric air layer, (3) the dust layer up to more than 5 km, and (4) the free troposphere. The MABL and the dust layer could be composed with different aerosol types (a mixture of sea salt, sulfate and possibly dust in the MABL) and the BER could then be different or comparable, depending on continental aerosol in the MABL as previously observed over the ocean during INDOEX for pollution aerosols [*Ansmann et al.*, 2000; *Pelon et al.*, 2002].

[12] The inversion of lidar data is described in Appendix A. It has been performed with the *Klett* [1981] algorithm and the MABL contribution is integrated as in the work by *Chazette et al.* [2001]. The determination of the extinction coefficient from lidar measurements needs the a priori knowledge of the aerosol backscatter to extinction ratio (BER), inverse of the so-called lidar ratio [e.g., *Pelon et al.*, 2002; *Chazette*, 2003]. Two ways have been considered to inverse LITE data. The first one is with a constant BER in the atmospheric column and the second one is with different values of BER in the PBL and the dust aerosol layer. In fact, spaceborne lidar measurements are affected by multiple-scattering [*Spinhirne*, 1982] and the BER derived is therefore an apparent backscatter to extinction ratio (ABER). This will be further discussed in section 6.

3. Dust Source Identification

[13] In order to investigate the transport and the source regions of the dust plumes seen by LITE, we have used Meteosat IR images and two other types of information derived from analyzed wind fields: air mass trajectories, and occurrences of surface wind speeds above the threshold allowing dust emission.

3.1. Meteosat Infrared Dust Index

[14] We have used low resolution (ISCCP-B2 subsampled resolution of 30 × 30 km^2 at nadir) IR images taken by Meteosat-5 at 1200 UTC to retrieve a dust index over continental Africa. Indeed, at midday an atmospheric dust layer causes apparent cooling, mainly because it significantly decreases the incoming solar light which warms the surface and also because it radiates in altitude at a cooler temperature than the hot surface [*Legrand et al.*, 1992]. On the basis of this property, *Legrand et al.* [1994] have defined the so-called infrared difference dust index (IDDI) by computing the difference between a given image and a reference (hot) image of the period. This index which they find correlated to the dust load, allows tracking the African dust clouds over Africa and source regions [*Marticorena et*

al., 1997, 2004; *Hamonou et al.*, 1999; *Brooks and Legrand*, 2000]. In order to tentatively distinguish possible source regions from transported dust clouds, we have selected IDDI values greater than 25 counts. This corresponds to an apparent cooling of ~10–12 K, to a column optical depth greater than ~1.5, and to a horizontal visibility below ~1 km or less [*Legrand et al.*, 2001]. Continental regions south of 30°N where the IDDI shows high turbidity between 12 and 17 September are highlighted in red in Figure 1. Very small spots most likely result from cloud contamination. Standard cloud tests defined for climatological studies have not been optimized here. The main dust source region appears as a wide area centered at (22°N, 2°W) in the Sahara desert (Mauritania, Mali, Algeria and western Niger) in agreement with the published maps of North African dust sources in September [*Marticorena and Bergametti*, 1996; *Prospero et al.*, 2002] or autumn [*Brooks and Legrand*, 2000]. The daily distribution of the daytime IDDI is illustrated for six days between 11 and 19 September in Figure 3, together with wind fields at 700 hPa. The circulation shows a high-pressure area over ocean in the northwestern part of the domain whereas westerly trade winds over the Saharan dust sources and the TAO explain the dust plume over the ocean observed in Figure 1.

3.2. Simulation of Dust Emission Occurrences

[15] Aeolian dust emissions from bare soils occur only when the surface wind exceeds a given threshold V_t which is a function of the aerodynamic surface roughness Z_0 and soil properties [*Gillette*, 1979]. The erosion threshold, 10-m wind velocity has been mapped for northwestern Africa [*Laurent*, 2005] following the approach described for China deserts in the work by *Laurent et al.* [2005]. It is based on a $0.25° \times 0.25°$ resolution data set of Z_0 derived from satellite [*Marticorena et al.*, 2004] and on a validated parameterization of V_t as a function of Z_0 [*Marticorena and Bergametti*, 1995; *Marticorena et al.*, 1997]. V_t values were compared with the surface wind velocities from the analyzed wind fields of the European Centre for Medium-range Weather Forecast (ECMWF). Latitudinal and longitudinal wind velocities at 10 m, at 0000, 0600, 1200, and 1800 UTC, were obtained with a resolution of $1.125° \times 1.125°$ from the CLIMSERV database (http://climserv.ipsl.polytechnique.fr). The horizontal wind velocity was interpolated on the $0.25° \times 0.25°$ grid. The likely source areas were then determined comparing the horizontal wind speed to the erosion threshold wind velocity. Regions where this difference is positive were then identified and cumulated for each day. They are delimited in Figure 3. Source regions identified by the IDDI and the wind fields do not always match. This can be due on the one hand to the cloud cover and to the low-IDDI masks applied to IR images, and on the other hand to errors in surface wind fields since even small variations in wind speed can trigger the source localization when the wind velocity is closed to V_t, which is generally of the order of 7–8 m s^{-1} in sandy deserts.

[16] A synthesis of the delimited dust source areas is shown in Figure 4. Early in the period, the dust emission occurs mainly in the region of Reggane in Algeria, around (26°N, 0°E) in the north of the main Saharan source area detected with the IDDI (Figure 1) and with TOMS [*Prospero et al.*, 2002]. This corresponds to the location where LITE shows aerosol close to the surface at night on the 12 September orbit (35). In the late period, dust emissions occur more southwesterly in the well known coastal source of western Sahara [*Marticorena and Bergametti*, 1996; *Prospero et al.*, 2002] and in the El Djouf region of northern Mali and Mauritania [*Brooks and Legrand*, 2000]. The locations of low-altitude aerosol layers detected on LITE data of 15, 17 and 19 September follow this displacement of dust emissions (Figure 4).

3.3. Trajectory Analysis

[17] Aerosol plumes have been observed with LITE around 0100 GMT. To investigate more precisely their origins, we computed air mass trajectories with the HYbrid Single-Particle Lagrangian Integrated Trajectory (HYSPLIT) model (http://www.arl.noaa.gov/ready/hysplit4.html). Depending on LITE observations, back trajectories ending at different altitude levels between 0.5 and 5 km above the mean sea level (amsl) were computed over 6 days. The choice of these levels was made to track aerosol layers observed by LITE over the top of the MABL.

[18] The back trajectories from 17 September back to 12 September are shown in detail. The location of starting point of trajectories (end point of transport) is reported in Figure 2. The horizontal projection of trajectories is plotted in Figure 1 and the vertical projection is given in Figure 5. These figures show that the dust observed at all levels above the marine atmospheric boundary layer on 17 September (orbit 115) is originating from the top of the Saharan dust layer formed by convection over land during daytime. The back trajectory for the lower level confirms a descent of free tropospheric air from the Atlantic between the MABL and the dust layer. This could be expected from the vertical structure seen at 20°W in Figure 2.

3.4. Discussion of Dust Sources

[19] Regarding upper levels on 17 September, the back trajectory at the bottom of the dust layer (1.5 km; Figures 1 and 2) shows that the transport is consistent with an origin from a dust source in the region of Reggane (Erg Chech, a source very often activated [*Marticorena et al.*, 1997]). This source was likely active on 12 September according to the dust emission model (contours in Figures 3b and 4). It roughly coincides with the dust uptake seen with LITE on orbit 35. The two other trajectories ending at 3 and 5 km are very close and highlight a transport slightly more in the south. However, the three trajectories are close enough to consider in the analysis that the dust particles at the different altitudes have the same source region. Moreover Figure 5 indicates that dust over the ocean on 17 September has the same age of 3–4 days in the different layers. Thus we assumed the same optical properties of dust at all altitudes in the column. We further assumed that the BER of dust was the same as that of dust observed in the dusty region of orbit 35 on 12 September, the source region of dust observed on 17 September. Size distribution changes are likely to occur close to the source regions because of the loss of the largest dust particles and this assumption could cause some bias in the lidar profile inversion over the source regions. Trajectories (not shown) ending at 3 and 5 km at (15°W, 17°N) in the other dust cloud transported in altitude at 15°W over Africa as shown in Figure 2, has likely close source regions

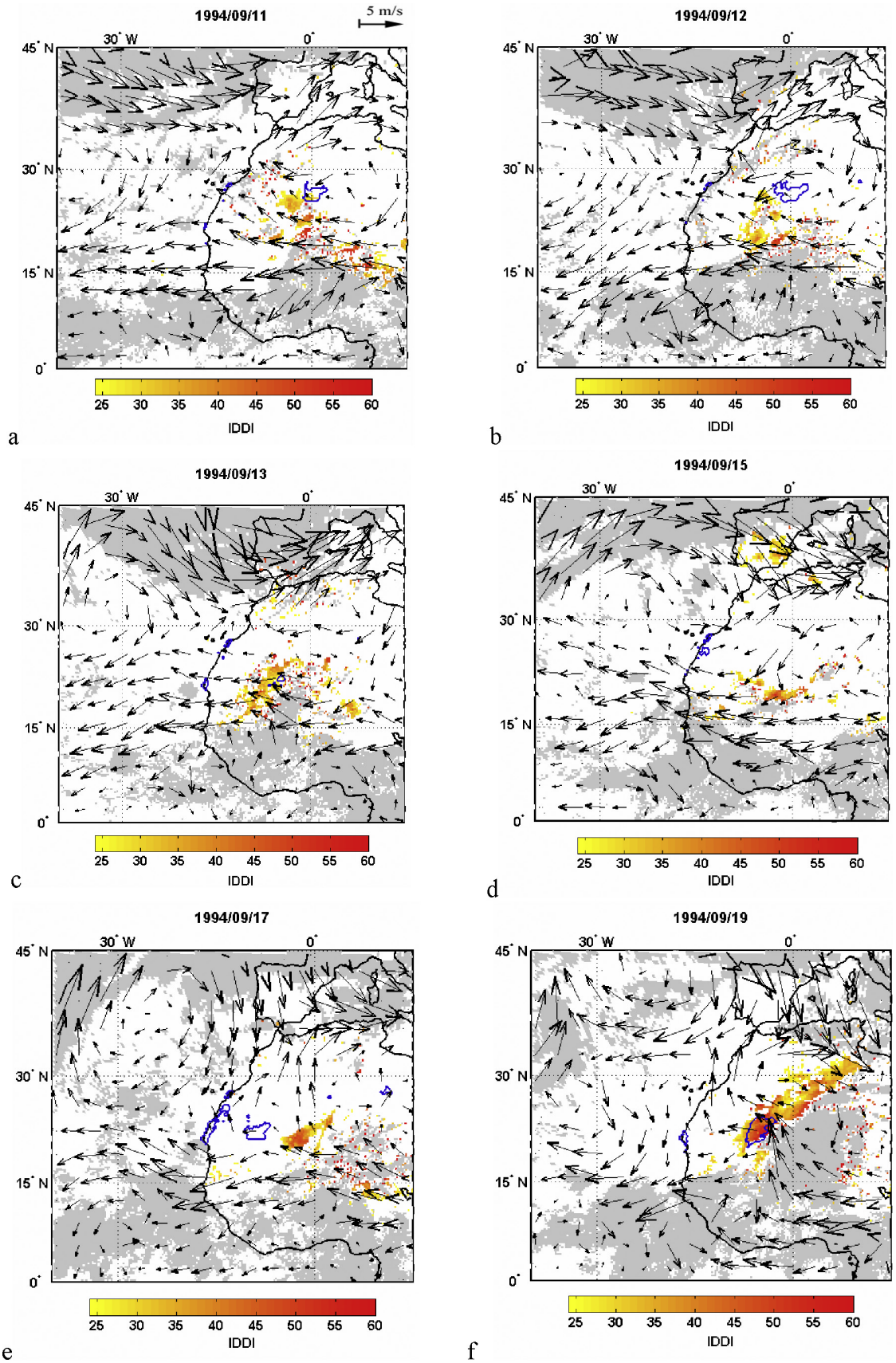
1994/09/11
5 m/s
30° W
0°
45° N
30° N
15° N
0°
25 30 35 40 45 50 55 60
IDDI
a
1994/09/12
30° W
0°
45° N
30° N
15° N
0°
25 30 35 40 45 50 55 60
IDDI
b
1994/09/13
30° W
0°
45° N
30° N
15° N
0°
25 30 35 40 45 50 55 60
IDDI
c
1994/09/15
30° W
0°
45° N
30° N
15° N
0°
25 30 35 40 45 50 55 60
IDDI
d
1994/09/17
30° W
0°
45° N
30° N
15° N
0°
25 30 35 40 45 50 55 60
IDDI
e
1994/09/19
30° W
0°
45° N
30° N
15° N
0°
25 30 35 40 45 50 55 60
IDDI
f

Figure 3

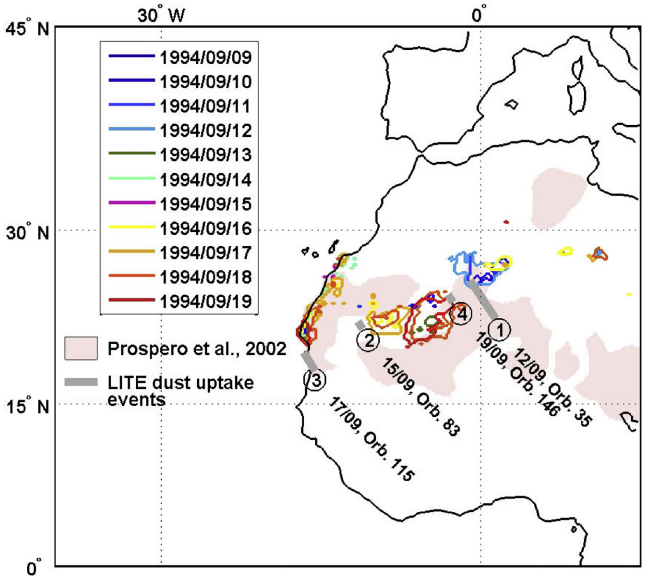

Figure 4. Simulation of the dust sources regions for each day of the LITE mission. For each day, all the slots (0000, 0600, 1200 and 1800 HTU) of ECMWF 10-m wind data are considered. Grey sectors give the location of the dust uptake as detected from LITE observations. Pale pink areas correspond to synthetic known sources of aerosols as given by *Prospero et al.* [2002]. Numbers 1 to 4 correspond to dust uptake event locations as observed with LITE data (see Table 1).

in the Erg Chech area. Emission events in this area seem to occur on 12, 17 and 19 September (Figures 3a, 3b and 3f, respectively). They are likely responsible for the dust events observed on orbits 35, 115 and 146. In the cases of orbits 35 and 146, dust uptakes take place the day of the passage of LITE in the west of Hoggar Mountains close to the Tanezrouft field (Figure 3c). The dust plume observed on orbit 84 is certainly related to the activity of a source located in El Djouf area. This area is identified on the wind field from ECMWF reported in the Figure 3c for 13 September. Sahelian sources (22°N, 5°W) also seem to have been active on Mali on 15 September (Figure 3d). They explain the lidar observations on orbit 147. The dust sources of the Moroccan (western Sahara) coast are also very active and could be at the origin of the dust events on orbits 83 (Figure 3c) and 131 (Figure 3e).

[20] We have made a comparable analysis using forward trajectories (not shown) computed with HYSPLIT model for some of the points of the LITE orbits that intercept the source regions and where clear air with dust aerosols was observed over land. Thus we have checked where they would end over the sea considering the same three altitude levels. All the trajectories finish in the dust plume highlighted in Figure 2 from Meteosat-5 observations. Hence the BER that can be retrieved over the TAO will be used to retrieve the vertical profile of the aerosol extinction coefficient from the LITE measurements over the desert.

[21] The main dust uptake regions identified from LITE data are reported in Figure 1 and listed in Table 1. All potential dust source areas identified by strong surface winds are shown in Figure 4. Source regions from LITE data and from Meteosat IR analysis are also reported on the same figure.

[22] A very good agreement is observed between the source areas determined from LITE data and from the dust uptake identification based on the comparison between ECMWF surface winds and *Vt* map. The comparison between the dust emission occurrence estimation and the results from Meteosat infrared radiances, however, shows a discrepancy about the aerosols uptake observed over the Tenere Desert (20°N, 13°E). This may be due to errors in the Meteosat analysis or to the occurrence of larger wind speeds than modeled. In the absence of lidar data it is not possible to conclude on either of the hypotheses. Nevertheless, it seems difficult to separate the contributions of dusts sources and transported dust using the Meteosat infrared information alone.

[23] Dust in the Mediterranean is known to be generally of a more northern origin [*Moulin et al.*, 1998]. The orbits in the Mediterranean Sea (orbits 129 and 145, Figure 2), show a tenuous AOD. Back trajectories (not shown) ending at all levels up to 5 km in the Gulf of Gabes and over northern Lybia come from the east and suggest transport from the well known source of northeast Algeria–south Tunisia [*Bergametti et al.*, 1989; *Moulin et al.*, 1998; *Prospero et al.*, 2002, Figure 5b; *Guieu et al.*, 2002], although this localization is not confirmed by Meteosat IDDI or dust uptake occurrence simulations. For the part of these two orbits in the western basin, back trajectories clearly indicate a northern origin and they will not be considered hereinafter. Indeed, at the island of Lampedusa (35.5°N, 12.6°E) *Di Iorio et al.* [2003] have found that dust and pollution particles can be observed and have different BER values.

4. Methodological Synergy Between LITE and Meteosat-5

[24] The nighttime LITE and middaytime Meteosat-5 data are used in this study to retrieve the BER values for aerosols over the Atlantic Ocean and Mediterranean Sea, assuming no significant change of properties between the two observation periods which are shifted by a maximum of 12 hours. The 700 hPa wind was used to position in the Meteosat image the dust parcel observed with LITE. It is expected that the high spatial homogeneity of dust plume permits the use of Meteosat-5 retrieved-AOT to be a constraint for the lidar inversion. Such a hypothesis will be discussed in the last section.

[25] Using the retrieved Meteosat AOTs at 550 nm as a constraint in the inversion procedure of the lidar signal at 532 nm, it is possible to determine the BER, inverse of the so-called lidar ratio [e.g., *Pelon et al.*, 2002; *Chazette*,

Figure 3. European Centre for Medium-Range Weather Forecasts (ECMWF) wind fields at 700 hPa for (a) 11, (b) 12, (c) 13, (d) 15, (e) 17 and (f) 19 September 1994. The IDDI from Meteosat-5 allows dust source identification (grey areas correspond to clouds). The potential dust uptake regions simulated by the emission model are also given (blue contours).

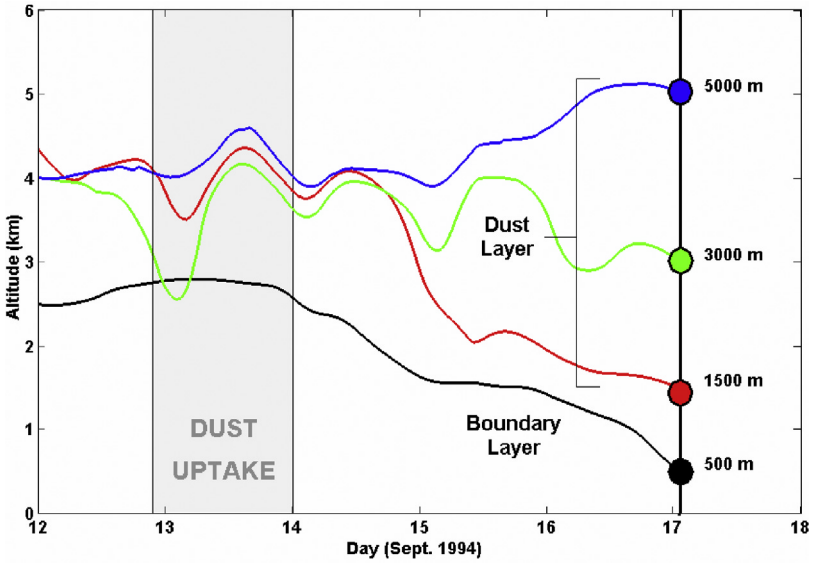

Figure 5. Air mass altitudes along the 6-day back trajectory (courtesy of NOAA Air Resources Laboratory http://www.arl.noaa.gov) ending at 0100 GMT (24.5°N–20.1°W). The black back trajectory starts at 500 m amsl, the red one starts at 1500 m amsl, the green one starts at 3000 m amsl, and the blue one starts at 5000 m amsl. Horizontal projections are shown in Figure 1.

2003]. The BER is corresponding to the product of the aerosol single scattering albedo and the aerosol phase function for backscattering. It is thus a function of the aerosol particle complex refractive index, size distribution, and shape. It can vary with altitude. To avoid a too large complexity we considered only two simplified models of aerosol vertical distribution over the ocean. The first one is assuming a constant BER in the atmospheric column and the second one is considering different values of BER in the MABL and in the dust aerosol layer. In fact, for space observations, multiple-scattering effect is also affecting the scattering of the propagating laser light. Indeed, depending on the system parameters and on the optical thickness of the scattering layer, spaceborne lidar observations are more or less perturbed by multiple scattering [*Eloranta*, 1972]. In the lidar equation this effect can be considered as changing the BER to an apparent BER defined by BER/η (see Appendix A) or the AOT to an a apparent AOT defined by the product $\eta \times$ AOT, where η is the multiple scattering factor (with $\eta < 1$ [*Platt*, 1981]). Hence the BER considered in the inversion is the apparent BER (ABER) including multiple scattering effects. Because of the large reception field of view (3 mrad for nighttime condition and 1 mrad for daytime condition), multiple scattering significantly increases the BER and has to be taken into account in the analysis procedure [*Eloranta*, 2002].

[26] In the first method of this study, which is the operational method of the CALIPSO mission, we assume that the ABER is constant throughout the atmospheric column as in the work by *Pelon et al.* [2002] or *Dulac and Chazette* [2003]. Such a hypothesis could be supported by the efficient mixing of the dust aerosol in the atmospheric column mainly due to both the uptake and the transport processes. Only the data acquired above the ocean have been used because the retrieval of AOT from Meteosat-5 radiance is not possible over land. The aerosol cloudless LITE data are first inverted with an initial value of the BER (arbitrary taken to be equal to 0.03 sr^{-1}). The lidar-derived integrated aerosol optical thickness is then compared with the Meteosat-5 AOT over the same oceanic region. The BER value is increased (resp. decreased) if $AOT_{lidar} - AOT_{Meteosat} > 0$ (resp. $AOT_{lidar} - AOT_{MET} < 0$). The convergence is achieved when the difference stays in the range of uncertainty linked to the Meteosat-5 retrieved AOT (25%). Such a procedure has been successfully applied by *Welton et al.* [2000], *Stephens et al.* [2001], *Pelon et al.* [2002], *Chazette* [2003], *Chazette et al.* [2005], and *Dulac and Chazette* [2003].

[27] For the second method, the altitude of the top of the MBL, which is directly given by LITE data, was integrated in the inversion process to separate the contribution of the two aerosol layers (Method 2). The value of the BER within the MBL layer is fixed to 0.041 sr^{-1}, a value established by *Flamant et al.* [1998] for marine aerosols (sea salt ans sulfate) over the open Atlantic Ocean, and which is affected by less than 5% by the multiple scattering for the magnitude

Table 1. Location of the Dust Aerosols Uptake Events as Reported From LITE Data

Event	Date	Orbit	Location	Latitude/Longitude
1	12 Sep 1994	35	Ould Mouloud (Algeria)	25.8°N, 1°W to 22.6°N, 1.4°E
2	15 Sep 1994	83	Rallaouya (Mauritania)	22.3°N, 11.5°W to 21.7°N, 10.1°W
3	17 Sep 1994	115	Nouakchott (Mauritania)	19.6°N, 16.6°W to 18°N, 15.5°W
4	19 Sep 1994	146	Tanezrouft (Algeria)	24.6°N, 3.1°W to 24°N, 2.7°W

Table 2. Dust Aerosol Observations From LITE Measurements in September 1994[a]

				Method 2		
Day	LITE Orbit	Meteosat AOT	Method 1, ABER, sr^{-1}	LITE DL AOT	LITE MBL AOT	ABER, sr^{-1}
12	35 (D_B)	0.17 ± 0.04	0.019 (8×10^{-3})	0.13 ± 0.04	0.036 ± 0.016	0.015 (7×10^{-3})
15	83 (D_A)	0.27 ± 0.09	0.019 (5×10^{-3})	0.25 ± 0.08	0.022 ± 0.019	0.018 (5×10^{-3})
15	84 (D_A)	0.52 ± 0.07	0.025 (3×10^{-3})	0.29 ± 0.05	0.227 ± 0.039	0.019 (5×10^{-3})
17	115 (D_B)	0.19 ± 0.06	0.013 (4×10^{-3})	0.15 ± 0.04	0.038 ± 0.029	0.009 (2×10^{-3})
17	115 (D_A)	0.50 ± 0.11	0.023 (4×10^{-3})	0.42 ± 0.10	0.077 ± 0.021	0.021 (4×10^{-3})
17	129 (D_B)	0.24 ± 0.05	0.021 (5×10^{-3})	0.17 ± 0.05	0.072 ± 0.031	0.015 (6×10^{-3})
18	131 (D_B)	0.18 ± 0.04	0.020 (5×10^{-3})	0.12 ± 0.03	0.050 ± 0.020	0.014 (5×10^{-3})
18	131 (D_A)	0.29 ± 0.07	0.028 (6×10^{-3})	0.21 ± 0.08	0.074 ± 0.022	0.025 (7×10^{-3})
18	145 (D_B)	0.33 ± 0.02	0.022 (5×10^{-3})	0.28 ± 0.03	0.051 ± 0.014	0.020 (5×10^{-3})
19	146 (D_B)	0.17 ± 0.02	0.021 (5×10^{-3})	0.11 ± 0.03	0.058 ± 0.015	0.013 (6×10^{-3})
19	147 (D_B)	0.17 ± 0.03	0.019 (6×10^{-3})	0.14 ± 0.03	0.022 ± 0.013	0.017 (6×10^{-3})
19	147 (D_A)	0.28 ± 0.12	0.027 (6×10^{-3})	0.21 ± 0.09	0.067 ± 0.041	0.025 (7×10^{-3})
12–19	(D_B)	0.20 ± 0.06	0.019 (6×10^{-3})	0.15 ± 0.05	0.046 ± 0.027	0.014 (6×10^{-3})
12–19	(D_A)	0.38 ± 0.15	0.024 (6×10^{-3})	0.31 ± 0.14	0.071 ± 0.044	0.023 (7×10^{-3})

[a]Measurements corresponding to Meteosat-5 AOT > 0.25 (<0.25) are noted as D_A (D_B). For each section of orbit where dust aerosols were present, the associated Meteosat total aerosol optical thickness (AOT), dust layer (DL) AOT, marine boundary layer (MBL) AOT, and the ABER derived from methods 1 and 2 are given with their standard deviations in parentheses. The last lines give the mean values derived from the synthesis of all dusty orbits.

of the optical thicknesses retrieved over the open ocean (see the following section). This second method thus allows us to estimate the ABER of the aerosols coming from continental sources, without including that of the marine aerosols trapped in the MBL.

[28] The two methods were applied to each LITE profile over ocean where dust particles were present. Two ABER values are thus retrieved for each profile where dust particles are present over the TAO.

5. Results

5.1. Apparent BER

[29] For the orbits presented in Table 2, the number of inverted LITE profiles with aerosol events is ~4100. (almost none above the Guinea Gulf because of the proximity of the convergence inter tropical zone which induces cloud coverage). The mean results of the ABER retrieved from the two inversion approaches are given for each orbit in Table 2.

[30] The analyzes were performed for dust aerosol events considering two types of aerosol mixing between the particle trapped in the MBL and the dust aerosol layer. The first one corresponds to the western coast of Africa, an area hereinafter noted D_A, where the main dust plume occurred and where the stronger value of AOT was registered. The optical contribution of dust particles is dominant in such an area. The main dust plume is located between 12°N and 27°N, and, −40°W and 14°W as shown in Figure 1. The orbits crossing this plume are the orbits 83, 84, 115, 131 and 147. The second type of aerosol mixing corresponds to other locations where the Meteosat-5 derived AOT is weaker (AOT < 0.25), hereinafter noted D_B.

[31] The mean BER value retrieved by the method 1 in area D_B, is about 0.019 ± 6.10^{-3} sr^{-1} corresponding to a mean AOT of 0.20 ± 0.06 at 532 nm (Table 2). In area D_A, the mean ABER seems to be smaller and close to 0.024 ± 6.10^{-3} sr^{-1} for a mean AOT of 0.38 ± 0.15 (Table 2). The first inversion of LITE profiles using method 1 shows the existence of two aerosol layers above the TAO or the Mediterranean Sea. These two layers could be composed with different aerosol types (sea salt, sulphate, dust) and the ABER could be then different against the altitude as previously shown by *Ansmann et al.* [2000] and *Sicard et al.* [2003]. The use of method 2 is then more appropriate to analyze such cases. After localization of the MBL top height following a procedure proposed by *Chazette et al.* [2002], the appropriate ABER has been applied to the MBL and the ABER of dust aerosols have been retrieved.

[32] The ABER values retrieved from method 2 for the aerosol in the free troposphere layer are reported in Figure 6 for all the inverted LITE profiles over the TAO. The values found highlight the boundaries of the dust plume over the TAO. The AOT in the MBL is larger in area D_A (0.071 ± 0.044) than in area D_B (0.046 ± 0.027) (Table 2). This may be due to a mixing of marine aerosol trapped in the MBL with dust particle in presence of convective cells generated by the stratocumulus clouds present in the studied region. Such a situation is well highlighted along the orbit 84 where the contribution of the MBL to the total optical thickness reaches more than 45% (MBL AOT ~ 0.23). In the other situations, this contribution is about 20% (MBL AOT < 0.08, very close to the value established over the open ocean by *Flamant et al.* [1998]).

[33] The mean ABER stays very similar between the two methods or at least in the error bars (Table 2). The most important differences are obviously observed when the contribution of the MBL to the total AOT is the highest. In the case of the orbit 84, the high MBL AOT (0.23) strongly suggests that dust particles are dominant in the MBL. This implies a BER value of MBL aerosol lower than the reference value assumed for marine aerosol. An estimation of the possible influence of the variable value of the BER in the MBL on the aerosol profile can be obtained by comparing results obtained from method 1 and 2 since method 1 assumes a constant BER in the vertical. Results from method 1 (Table 2) indicate that if a value of 0.025 sr^{-1} is used rather than the value of the marine aerosol model (0.041 sr^{-1}), the derived dust BER is found equal to 0.025 sr^{-1} instead of 0.019 sr^{-1}. This suggests that a maximum bias of 30% in dust BER may be due to the variability of the BER in the MBL in the case of dust predominance in the MBL. On the opposite case of orbit 115 where the dust layer is dominating the column AOT,

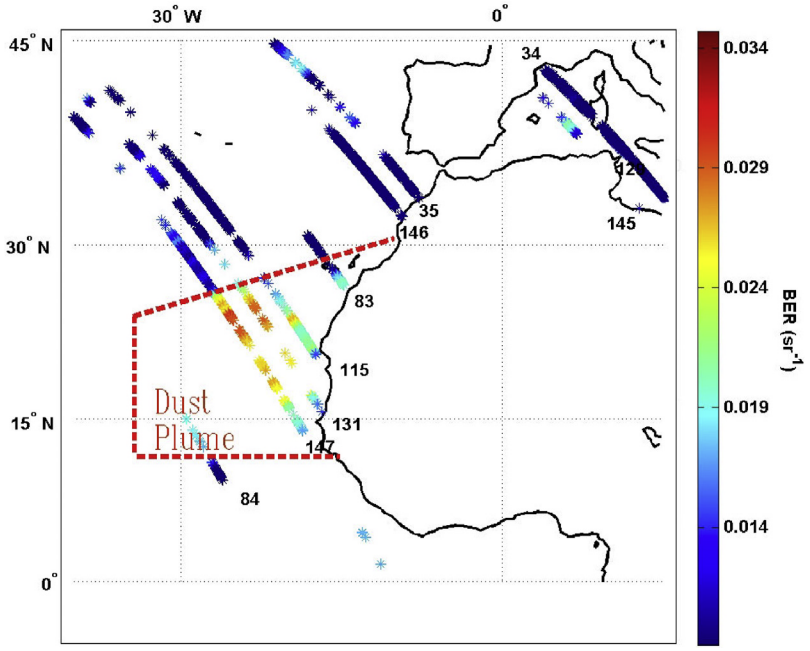

Figure 6. Aerosols ABER value retrieved over both the TAO and the Mediterranean Sea with the coupling of LITE and Meteosat observations. The main dust plume observed over the TAO during the period is highlighted.

assuming a value of 0.023 s^{-1} for the MBL aerosol would only slightly change the dust BER from 0.021 to 0.023 sr^{-1}. Over the Mediterranean (orbits 129 and 145), the presence of anthropogenic carbonaceous aerosol might cause values of the BER of MBL aerosol as low as ~0.020 sr^{-1} [*Dulac and Chazette*, 2003] which would yield an increase in dust ABER, from 0.020 sr^{-1} to 0.022 sr^{-1} in the case of the orbit 145, and from 0.015 sr^{-1} to 0.021 sr^{-1} in the case of the orbit 129.

[34] The mean value of the ABER of dust from method 2 is close to 0.023 sr^{-1} with a standard deviation ~7×10^{-3} sr^{-1}. This corresponds to lidar ratios of ~40 ± 13 sr. Comparable values are reported for dust over Africa [*Cattrall et al.*, 2005]. This value is thus also used to inverse the LITE data over land.

5.2. Lidar-Derived AOT and Extinction Coefficient

[35] The mean value of the ABER previously retrieved from method 2 (0.023 sr^{-1} for dust) was used to assess the aerosol vertical profile of extinction coefficient over continent. About 3000 cloud-free lidar profiles can be inverted over the continent. Indeed, spaceborne lidar offers the possibility to retrieve the AOT over continent in presence of high surface albedo (arid and semiarid surfaces) since the lidar signal is only contributed by the atmosphere. Figure 7 gives the dust AOT retrieved from LITE data over the sea and the African continent. The good continuity in AOT between the continent and the sea qualitatively validates the choice of the ABER. The mean value of the dust AOT assessed over the continent is 0.39 at 532 nm with a standard deviation of 0.10.

[36] The mean profiles of the aerosol extinction coefficients above continent, TAO and Mediterranean Sea are given in Figure 8. These profiles have been calculated for the different areas shown in Figure 7. These areas have been selected to sample the aerosol plumes over both ocean and continent. The variability in the aerosol extinction coefficient retrieval when the values of ABER $- \sigma_{ABER}$ and ABER $+ \sigma_{ABER}$ are used to inversed the lidar profiles are also considered. They define the colored area around the mean profiles shown in Figure 8. Despite this spread, the different structures observed on the profiles are always highlighted and the differences between profiles from different areas remain significant.

[37] The dust plumes observed close to the western part of the African continent gives the opportunity to follow the contrast between the profiles over the continent and the ocean (Figures 8a–8d). Over the northwestern African continent the dust layer extends up to 5 km amsl. For all cases the behavior is obviously very similar with significant separation between the MBL and the dust layer when air masses are advected over ocean. Such separation leads to the creation of a well defined aerosol vertical structure that can be transported over long distances, as already observed [e.g., *Hamonou et al.*, 1999; *Chazette et al.*, 2001; *Ansmann et al.*, 2003]. The altitude range of the dust transport is characteristic of the Saharan Air Layer identified by *Carlson and Prospero* [1972] that exists during summertime. Nevertheless, it seems as previously mentioned (Table 2) that the MBL may contain a mixing of dust and marine aerosols because significant values of extinction are observed in the MBL on some profiles (Figure 8a). Indeed, the classical MBL structure over the open ocean is closer to the one of Figure 8g. Note that a possible weak residual dust layer may be observed on this mean vertical profile between 3 and 5 km amsl. The lidar vertical profile calculated for the area F shows a peak of ~0.4 km^{-1} around 4 km amsl, which may be due to a cloud formation (Figure 8c). Such a

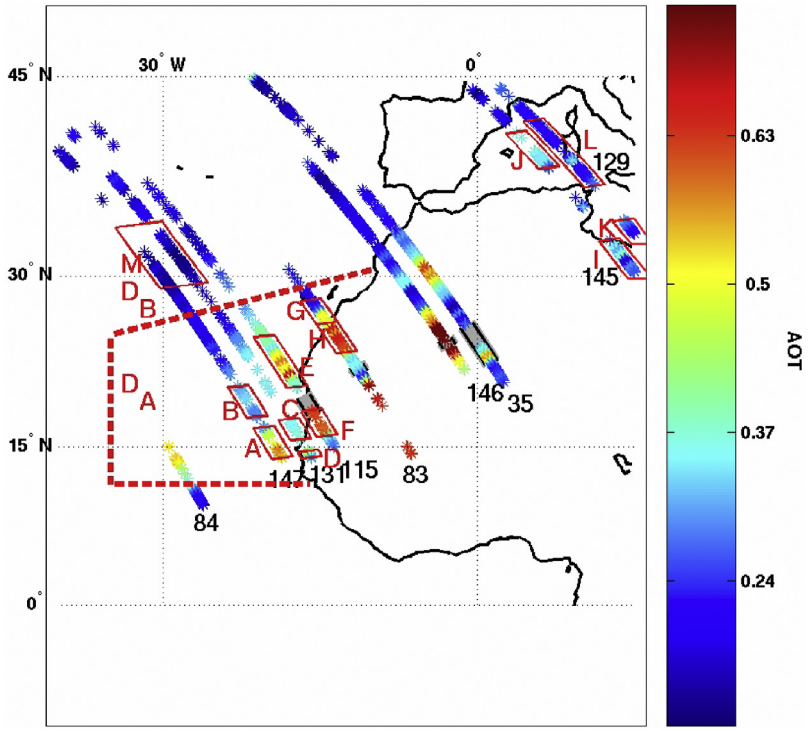

Figure 7. AOT retrieved after inversion over the TAO, the Mediterranean Sea and the continent. Grey sectors on the orbits give the location of the dust uptake as detected from LITE and Meteosat-5 data. The main dust plume observed with Meteosat over the TAO during the period (Figure 2) is highlighted. The letters from A to M indicate the areas where the mean LITE profiles have been inverted.

shape is not observed for the area H that is also very close to the dust source (Figure 8d).

[38] The selected areas in the Mediterranean region are associated with smaller dust loads but present similar behavior as the situations previously described for West Africa (Figures 8e and 8f), and by *Hamonou et al.* [1999]. The extinction coefficient profiles of dust particles show a lesser vertical extent of the aerosol over land in Figure 8e.

6. Discussion on the Lidar-Retrieved Parameters

[39] The main source of error in AOT over land is expected to come from uncertainties in the BER values used for the lidar data inversion. Errors on AOTs and on aerosol extinction coefficients can thus be related to several independent main causes [*Klett*, 1981, 1985; *Pelon et al.*, 2002]: (1) the uncertainty on the boundary condition at a reference altitude where the atmosphere is assumed molecular (see Appendix A) and the uncertainty on the a priori knowledge of the vertical profile of the Rayleigh backscatter coefficient as determined from ancillary measurements or atmospheric model interpolation, (2) the statistical fluctuations of the measured signal associated with random detection processes, (3) the uncertainty on the Meteosat-5 derived AOT, (4) the uncertainty due to the horizontal resolution of Meteosat-5, (5) the uncertainty due to the multiple scattering effect, and (6) the uncertainty due to the temporal synchronization between LITE and Meteosat-5.

6.1. Boundary Condition

[40] The boundary condition defined in equation (A2) of Appendix A assumes the existence of an aerosol free layer above the aerosol plume. The total backscatter coefficient β is then assumed due to the Rayleigh molecular contribution only. Such an assumption is relevant in our study for altitudes higher than 5 km amsl. The molecular contribution is derived from an ancillary climatic radiosounding database as in the work by *Chazette* [2003]. It was compared with the Rayleigh contribution calculated and interpolated following the altitude from the ECMWF thermodynamic vertical profiles corresponding to the LITE mission period. The effect of these two previous uncertainty sources on the optical properties of aerosols is negligible compared to the others (less than 2%).

6.2. Lidar Signal

[41] In clear sky condition the mean signal-to-noise ratio (SNR) was assessed on the LITE profile to be ~5.1 at the top of the aerosol layers during nighttime with a vertical resolution of 15 m. We computed this value using the mean values and the standard deviations calculated on consecutive groups of ~100 lidar profiles. The effect of the lidar signal noise was assessed using a Monte Carlo approach as used by *Chazette et al.* [2001]. A synthetic atmosphere was first considered on the basis of which different statistical realizations of the raw lidar signal were calculated including molecular and aerosol signature. The aerosol layer was considered to be ranging between altitude 0.5 to 5 km height, with an AOT equal to 0.31 and an initial BER of 0.023 sr^{-1}. Such values have been chosen following the previous results given in Table 2. The final distribution of the retrieved BER is obtained from 1000 random realizations that ensure a normal distribution around the lidar signal mean value.

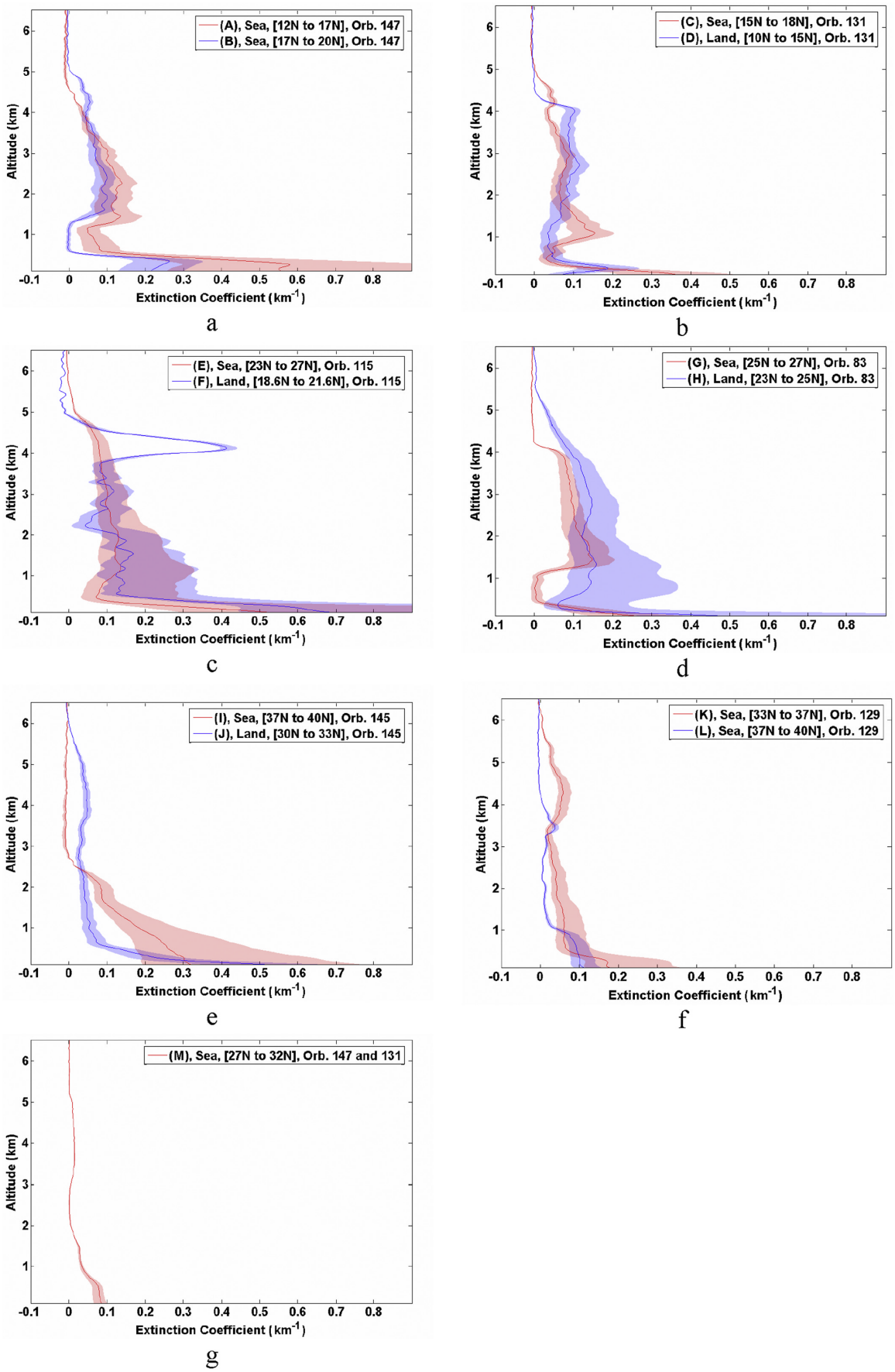
(A), Sea, [12N to 17N], Orb. 147
(B), Sea, [17N to 20N], Orb. 147
Altitude (km)
Extinction Coefficient (km-1)
a
(C), Sea, [15N to 18N], Orb. 131
(D), Land, [10N to 15N], Orb. 131
Altitude (km)
Extinction Coefficient (km-1)
b
(E), Sea, [23N to 27N], Orb. 115
(F), Land, [18.6N to 21.6N], Orb. 115
Altitude (km)
Extinction Coefficient (km-1)
c
(G), Sea, [25N to 27N], Orb. 83
(H), Land, [23N to 25N], Orb. 83
Altitude (km)
Extinction Coefficient (km-1)
d
(I), Sea, [37N to 40N], Orb. 145
(J), Land, [30N to 33N], Orb. 145
Altitude (km)
Extinction Coefficient (km-1)
e
(K), Sea, [33N to 37N], Orb. 129
(L), Sea, [37N to 40N], Orb. 129
Altitude (km)
Extinction Coefficient (km-1)
f
(M), Sea, [27N to 32N], Orb. 147 and 131
Altitude (km)
Extinction Coefficient (km-1)
g

Figure 8

Table 3. Error Sources on the BER in Terms of Standard Deviation[a]

Error Source	Standard Deviation
Standard deviation on the retrieved BER of dust over ocean (σ_{BER}, sr^{-1})	7×10^{-3}
σ_{BER} due to error on the LITE signal (SNR = 5.1)	1.9×10^{-3}
σ_{BER} due to the error in Meteosat-derived AOT ($\sigma_{AOT,Dust} = 7.7 \times 10^{-2}$)	4.3×10^{-3}
σ_{BER} due to multiple scattering	3×10^{-3}
Total σ_{BER}	5.6×10^{-3}

[a]Unit is sr^{-1}. The first line of the table gives the standard deviation in BER retrieved from the inversion of all LITE data over ocean. The three following lines correspond to simulated standard deviation in BER, considering separately the three main sources of errors. The last line gives the quadratic sum of these three errors.

[42] Results are reported in Table 3 for dust aerosols. The values of the standard deviation on ABER are between 10^{-3} and 1.9×10^{-3} sr^{-1}. The cases for different SNR have been also analyzed and reported in Figure 9. The SNR of the spaceborne lidar of the GLAS mission [*Zwally et al.*, 2002] has also been assessed to be close to 1.3 for the wavelength of 532 nm during nighttime for a vertical resolution of 75 m. The uncertainty on the ABER becomes very important with such level of signal-to-noise ratio. According to system specifications, the vertical profiles of the Cloud-Aerosol LIdar with Orthogonal Polarization (CALIOP) on board the CALIPSO satellite should be obtained with a better SNR that can be assessed to be close to 2.7 during nighttime for a vertical resolution of 15 m. It is reasonable to think that the performances of the CALIOP system will be close to the ones of the LITE system during nighttime.

6.3. Meteosat-Derived Optical Thickness

[43] In order to estimate the influence of the error on Meteosat-retrieved AOT a Monte Carlo approach has been also used. The random realizations were done considering a normally distributed AOT around 0.31 and the relative standard deviation on Meteosat-retrieved AOT of 25% [*Moulin et al.*, 1997a].

[44] The standard deviations on ABER are close to 4.3×10^{-3} sr^{-1}. They are greater than the ones due to the SNR by a factor of ~2. The use of more precise AOT products from the new generations of passive sensors such as Meteosat Second Generation (MSG, http://www.esa.int/SPECIALS/MSG/), Moderate Resolution Imaging Spectroradiometer (MODIS, http://modis.gsfc.nasa.gov/) and POLarization and the Directionality of the Earth's Reflectances (POLDER, http://smsc.cnes.fr/POLDER/) on board the Polarization and Anisotropy of Reflectances for Atmospheric Sciences coupled with Observations from a Lidar (PARASOL, http://smsc.cnes.fr/PARASOL/index.htm) will be a great advance to improve the synergy between spaceborne lidar and passive instruments.

[45] Figure 9 gives also the standard deviation on the ABER against the uncertainty in AOT of dust aerosols. The retrieval of the aerosol optical thickness have been significantly improved between the work of *Moulin et al.* [1997b] on Meteosat where the error on the AOT was close to 0.1 and the one of *Remer et al.* [2001] on MODIS where this error decreases to 0.02 over ocean. *Chu et al.* [2002] give an error between 0.05 and 0.2 for aerosol over the land retrieved from MODIS measurements at 470 nm. Intermediate errors are given by *Stowe et al.* [1997] using the Advanced Very High Resolution Radiometer (AVHRR) and by *Deuzé et al.* [1999] using POLDER (at 865 nm) with values close to 0.04 and 0.05, respectively, over ocean. The improvement of the AOT retrieval for the new generation of passive spaceborne instruments will conduct to a very significant decrease on the BER error. Indeed, as illustrated in Figure 9, when the AOT standard deviation decreases from 0.1 to 0.02 the standard deviation on the ABER decreases from ~0.005 to less than 0.001 for dust aerosols. Errors on ABER values given in Figure 9 are thus much smaller than the observed dispersion (0.01 sr^{-1} corresponding to a 50% change). This may be attributed to the different origins and/or size distributions of the dust particles, and needs further investigations.

6.4. Horizontal Resolution of Meteosat-5

[46] The Meteosat-5 data were used in the high-resolution mode of 2.5×2.5 km^2 (i.e., $0.02° \times 0.02°$). We degraded this resolution down to 48×48 km^2 to analyze the effect of a change in the horizontal resolution on the ABER retrieval. It turned out that the Meteosat-5 horizontal resolution has a weak influence on the retrieval of the ABER. This is mainly due to the homogeneous properties of the dust plume. Changing the resolution had no effect on the mean ABER value retrieved. It only affected the standard deviation in ABER which increased by $\sim 3 \times 10^{-4}$ sr^{-1} in the lower resolution. In such situations, the passive instrument horizontal resolution is not limitative.

6.5. Multiple Scattering

[47] The effects of the multiple scattering on spaceborne lidar signal must be considered [*Spinhirne*, 1982; *Grant et al.*, 1997]. Indeed, with a field of view between 1.1 and 3.5 mrad and an orbit at ~260 km amsl [*Winker et al.*, 1996], the atmospheric volume sampled by LITE was large enough to generate significant multiscattering photons that leads to an apparent reduction of the aerosol extinction coefficient. To consider the multiple scattering effect, a simple modification of the lidar equation was proposed by Platt [*Platt*, 1973, 1981]. A reduction factor η is introduced to the extinction coefficient in the exponential term of the lidar single scattering equation (see Appendix A). *Nicolas et al.* [1997] showed that this scheme is correct for the case of lidar sounding of a cirrus cloud, but may be only an approximation in the general case. Nevertheless, this

Figure 8. (a–g) Mean vertical extinction profiles of dust aerosols retrieved over different areas (A to M) shown in the Figure 6. The shaded areas represent the variability of the extinction coefficient linked to the uncertainty in the ABER.

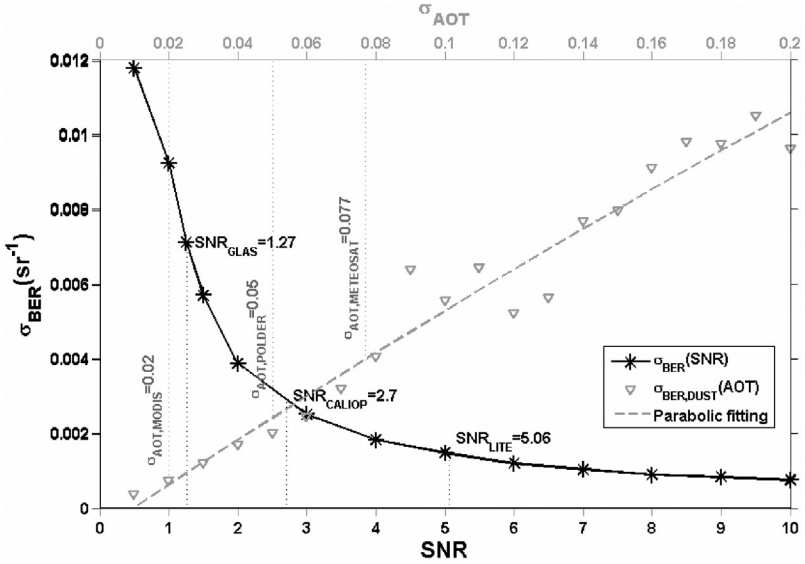

Figure 9. Standard deviation on the retrieved ABER against the lidar signal-to-noise ratio (SNR) and the standard deviation on the AOT. The SNR conditions of LITE, GLAS and CALIPSO missions are indicated. The standard deviations associated to the AOT retrieval from MODIS, POLDER and Meteosat-5 are also indicated.

approach has been used hereinafter to assess the effect of multiscattering in the aerosol plumes previously described.

[48] A value of 0.682 for η has been proposed by *Wiegner et al.* [1996] for the dust plume observed from LITE on the basis of a Monte Carlo study. *Karyampudi et al.* [1999] give values of η between 0.6 and 0.9. Nevertheless, information about the AOT dependence of η is missing and must be assessed. Hence we also used a Monte Carlo approach to model η and determine the number of multiscattering photons in a homogeneous dust layer between 0 and 5 km amsl. The number of photon realizations was 10^6. The multiple scattering factor η at different depths in the aerosols layer is then deduced from the ratio between the total lidar signal S (including single and multiple scattering S_{mul}) and the number of single-backscattered photon (see Appendix A).

[49] As shown in Figure 10, the value of η seems to vary significantly against AOT and then against the penetration depth in the dust plume. The range of variability proposed by *Karyampudi et al.* [1999] is coherent with our results for the dust AOT encountered during the LITE mission. If the values of η are supposed to vary between 0.6 (AOT $\sim$ 0.40)

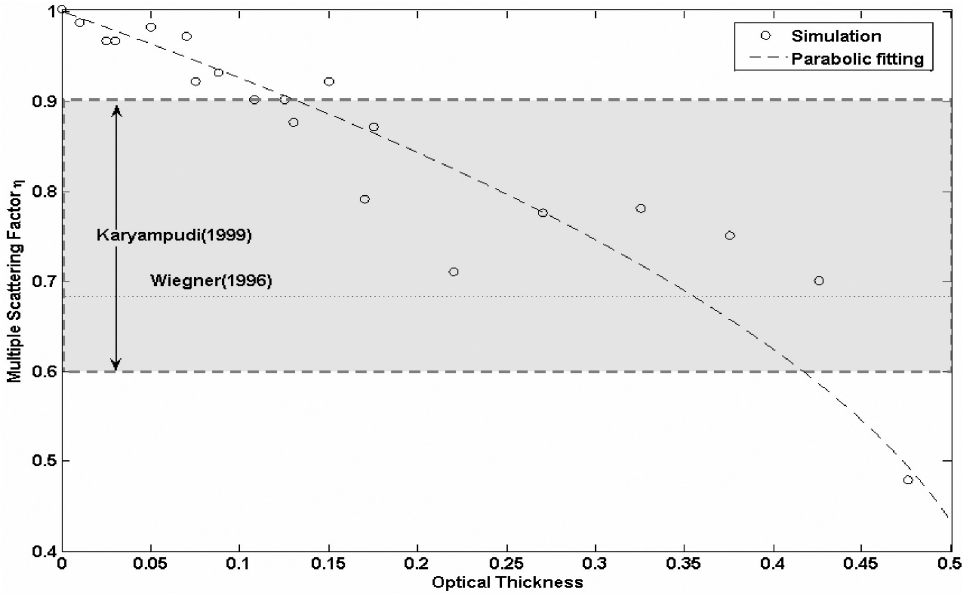

Figure 10. Distribution of the multiple scattering factor η retrieved from a Monte Carlo method against the altitude for a dust aerosol layer between 0 and 5 km amsl. The values proposed by *Wiegner et al.* [1996] (dotted line) and *Karyampudi et al.* [1999] (shaded area) are also given.

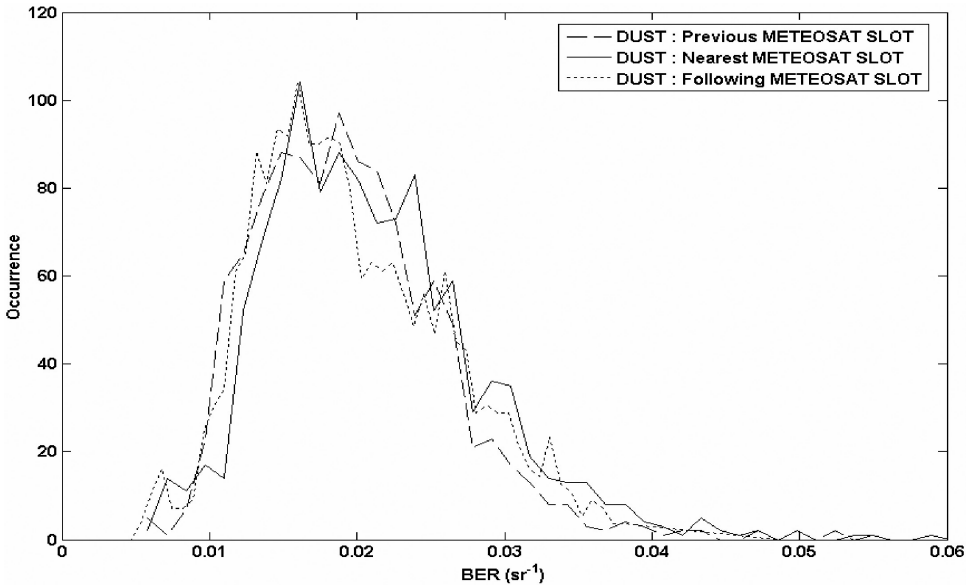

Figure 11. Probability density function of the Aerosols BER retrieved with method 2 over the TAO for dust aerosols. The calculations were performed for the previous, following and nearest Meteosat-5 observations.

and 0.9 (AOT $\sim$ 0.2) they lead to standard deviations of 3×10^{-3} and 1.7×10^{-3} sr^{-1}, respectively, on the retrieved BER.

[50] Figure 11 gives the histogram of BER after correction of the multiple scattering for each lidar profile. The mean value of the BER for the dust aerosol is close to 0.017 sr^{-1} with a standard deviation $\sim$0.006 sr^{-1}. The lidar ratio is then $\sim$57 $\pm$ 27 sr. This value could be compared to the results of *Cattrall et al.* [2005] that studied the variability of the lidar ratio against the aerosol type from some selected AERONET stations. Indeed, these authors found lidar ratio between $\sim$30 and 60 sr for the dust aerosol. *Chazette et al.* [2001] computed a value of 0.035 sr^{-1} from Mie calculations in the Azores region. During a Saharan dust episode over the Canary Islands *Powell et al.* [2000] and *Welton et al.* [2000] derive a BER of 0.029 $\pm$ 0.004 and 0.027 $\pm$ 0.007 sr^{-1}, respectively. However, during a Saharan outbreak off West Africa *Léon et al.* [2003] derive lower values of 0.018 and 0.024 $\pm$ 0.007 sr^{-1} in dust layers between 0.7 and 2.1 km amsl and 2.2 and 4.5 amsl, respectively. *Mattis et al.* [2002] used the Raman lidar technique to measure the BER value of elevated dust layers during two episodes over Germany. They report BER values between 0.013 and 0.025 sr^{-1}. *Liu et al.* [2002] and *Murayama et al.* [2003] also report layer averaged BER in ranges 0.018–0.024 and 0.022–0.025 sr^{-1}, respectively, for Asian dust over Japan. Note that higher values retrieved from Mie computations for dust particles can in fact be attributed to nonsphericity effects [*Liu et al.*, 2002; *Mattis et al.*, 2002]. Thus *Barnaba and Gobbi* [2001] compute smaller values of 0.020–0.028 sr^{-1} at 500 nm for nonspherical dust aerosols.

6.6. Temporal Synchronization

[51] Meteosat-5 and LITE observations were not performed at the same time. A significant bias could be induced on the BER retrieval if the aerosol plume significantly evolves between the two measurements separated by almost a half day. To evaluate such an effect three different constraints using Meteosat-retrieved AOT have been applied to inverse the lidar profiles. The first one was with the Meteosat observations from the day before the considered LITE measurement. The second one was with the Meteosat observations from the day after the LITE measurement. The third one was with the Meteosat observations closer in time from the LITE measurements. Figure 11 compares the results on the retrieval of the ABER. The differences are weak. Both the mean value and the standard deviation of ABER stay about the same. This proves that the aerosol plumes are very stable in time between the noon measurements of Meteosat and the nocturnal observations of LITE. Consequently, the temporal synchronization between LITE and Meteosat is not a major error source in the frame of our coupling study, since the LITE observation location can be approximately positioned on the Meteosat image using wind information.

7. Discussion on the Aerosol Radiative Impact

[52] The BER variability has a direct influence on the retrieved dust aerosol optical properties and thus on the determination of the aerosol radiative forcing at both the surface and the tropopause. To evaluate uncertainties on the retrieval of radiative forcings of the desert aerosols due to BER standard deviations we used the radiative transfer model Streamer developed by *Key and Schweiger* [1998], and *Key* [2001]. This model was used before to assess the radiative impact of the aerosols trapped in the monsoon plume following the INDOEX international campaign [*Léon et al.*, 2002].

[53] We run the model with surface emissivities of 0.98 for oceanic surfaces [*Liu et al.*, 1987] and of 0.90 for desert surfaces [*Ogawa and Schmugge*, 2004]. Spectral reflectances were taken for desert surfaces according to *Tanré et al.*, [1986] and for oceanic surface according to *Briegleb et al.*

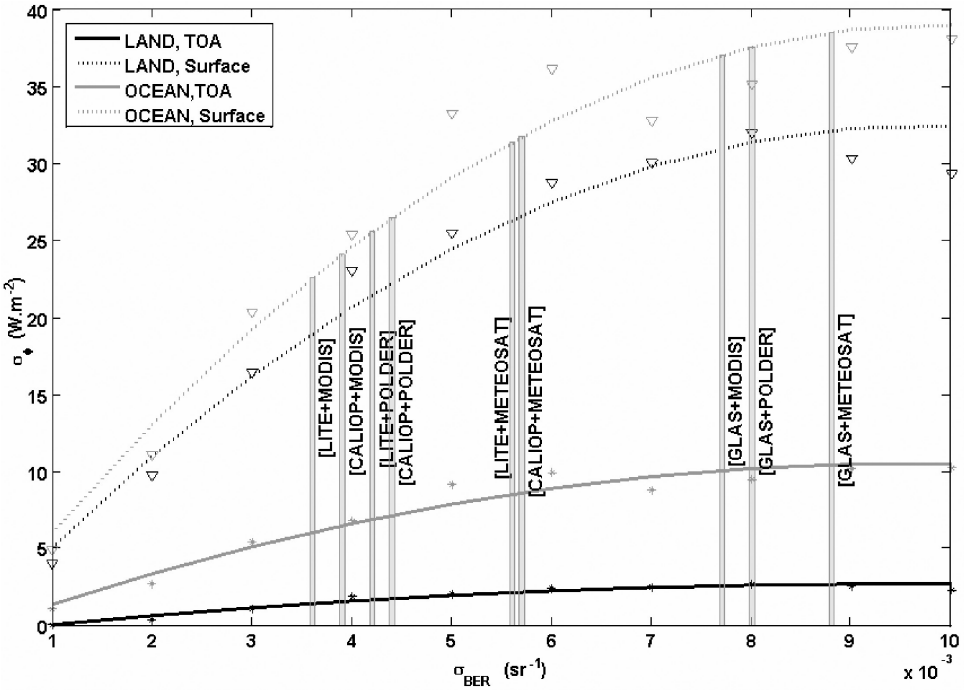

Figure 12. Standard deviation of the dust aerosol radiative impact (σ_ϕ) against the standard deviation on the BER (σ_{BER}) associated with different instrumental synergies.

[1986]. The profiles of temperature, water vapor and ozone were taken from ECMWF data corresponding to the observation period of LITE. The concentrations of the other main greenhouse gases which have a major influence on the radiative forcing were taken constant and with the default values of the Streamer model. The complex refractive index of the dust aerosols were taken according to *Volz* [1973]. The forcing was computed as the difference between simulations in clear sky and dust conditions. In order to assess dust differential radiative impact between desert and oceanic surfaces, we arbitrarily chose to use the same average extinction profiles of the Figure 8d which were taken on LITE orbit 83. The average profile corresponds to an optical thickness at 532 nm of 0.31.

[54] The direct radiative forcing is approximately -40 (-46) and approximately -8 (-18) W m^{-2} at the surface levels and at the tropopause, respectively, for the desert (oceanic) surface. The mean heating rate in the aerosol layer is then close to 0.45 (0.40) K/day. Figure 12 plots the standard deviations on the mean daily aerosol radiative forcing against the standard deviations on the BER. Relative errors are greater at the surface ($\sim$80% at the maximum) than at the tropopause (35–60% at the maximum). The BER standard deviations associated to various possible pairs of spaceborne lidar system and radiometer configurations were considered and the associated standard deviations on the dust radiative forcing are shown in Figure 12. It is clear that for all the passive radiometers coupled with the GLAS lidar, standard deviations on the radiative forcing assessment are most important because of the weak signal-to-noise ratio associated with this instrument. One reaches standard deviations of $\sim$30 ($\sim$40) and $\sim$3 ($\sim$10) W m^{-2} at the surface and tropopause levels, respectively, for desert (oceanic) surfaces. The use of the LITE system is the most accurate especially if coupled with MODIS, with values lower than 20 (23) and 2 (6) W m^{-2} at the surface and tropopause levels, respectively, for desert (oceanic) surfaces. Assuming expected performances of the CALIOP system, its results will be little degraded compared to LITE. In the near future, the CALIOP and MODIS synergy should yield the most accurate results on aerosol radiative forcing with standard deviations of $\sim$20 ($\sim$24) and $\sim$1.6 ($\sim$6.5) W m^{-2} at the surface and tropopause levels, respectively, for desert (oceanic) surfaces.

8. Conclusion

[55] Inversion methods used to analyze lidar data need to be constrained to allow accurate retrievals of aerosol optical properties. One of the key parameters required is the aerosol backscatter-to-extinction ratio (BER). However, it depends on the aerosol size distribution, complex refractive index and particle shapes. It is often not possible to directly determine all parameters but necessary to know both the aerosol origin and the processes of transport to select an a priori aerosol model. The synergy between active and passive remote sensing instruments gives the possibility to retrieve the aerosol optical properties in a more accurate way.

[56] The synergy between the LITE lidar system and Meteosat passive sensor has been used to constrain the retrieval of the vertical distribution of aerosols over high surface albedo (arid and semiarid surfaces) using back trajectory analysis.

[57] Meteosat offers the possibility to assess the dust aerosol optical thickness over oceans. This information combined with lidar data was used to constrain the retrieval of the vertical distribution of aerosols and thus to determine the ABER following two methods. In the first method the ABER was assumed to be constant throughout the atmo-

spheric column and in the second method the contribution of the MBL was separated from the one of the dust aerosol layer. The difference between the two methods is not significant as it stays in the error bars. The influence of the multiple scattering on the retrieved ABER is shown to be important. Values of the multiple scattering correction factor η of $\sim$0.6 and $\sim$0.8 have been assessed for AOT of $\sim$0.4 and $\sim$0.2, respectively. After correction of the multiple scattering factor, the values of BER for the dust aerosols (region D_A) have been shown to vary by more than a factor of 2, from $\sim$0.01 to $\sim$0.03 sr^{-1}. The total standard deviation σ_{BER} on the retrieved BER has been assessed to be equal to 5.6×10^{-3} for the dust aerosol for a mean value close to 0.017 sr^{-1}. These values are close to the values reported in the literature [*Cattrall et al.*, 2005].

[58] Using the ABER retrieved over the TAO, vertical profiles of dust aerosol extinction coefficient have then been retrieved over Africa. Such an approach allowed us to retrieved high values of optical thicknesses in areas where passive sensors alone would not allow their determination. It is then a new insight to monitor the aerosol vertical distribution over continents and better understand their radiative forcing and their impact on dynamics.

[59] We have shown that the half day time lag between passive and lidar observations is not a major source of uncertainty when aerosol plumes are well established. Such an approach is a first step in the perspective of the future synergies that could be used for the new generation of spaceborne instruments as MSG (http://www.esa.int/SPECIALS/MSG/), MODIS (http://modis.gsfc.nasa.gov/) and POLDER on board PARASOL (http://smsc.cnes.fr/PARASOL/index.htm). Multispectral observations using the additional near infrared channels from both sensors [*Kaufman et al.*, 2003] and polarization analysis from CALIOP on board CALIPSO will offer new observational capabilities allowing improvement of the lidar inversion procedure. From a sensitivity study we have shown that the assessment of the BER may be carried out with standard deviations close to 0.003 sr^{-1} (0.004 sr^{-1}) using the expected synergy between CALIOP and MODIS (CALIOP and PARASOL). Such a synergy may lead to a significant assessment of the dust aerosol direct radiative forcing at both the surface and the tropopause levels. Nevertheless, the uncertainty remains high ($\sim$50%) mainly because of both the signal-to-noise ratio of spaceborne lidar measurement and the uncertainty on the BER. A significant improvement can be obtained for the homogeneous aerosol layers which make it possible to average several coincident lidar and passive spaceborne observations in order to improve the signal-to-noise ratio.

[60] The international experimental program African Monsoon Multidisciplinary Analysis (AMMA, http://amma.mediasfrance.org/) will be an ideal frame where the spaceborne synergy between lidar and passive radiometers will offer the possibility to improve the scientific knowledge about the dust and biomass impact on both the tropical dynamic and water cycle.

Appendix A: Lidar Signal Inversion

[61] For spaceborne measurements, the lidar equation gives the range-corrected signal S(z) for the emitted wavelength of 532 nm as a function of the range z, the pointing angle θ, the total backscatter β(z) and extinction coefficients α(z) [*Measures*, 1984]:

$$S(z) = C \cdot \beta(z) \cdot \exp\left[-2/\cos(\theta) \cdot \int_z^{z_s} \alpha(z') \cdot dz' \right] \tag{A1}$$

where z_s is the altitude above the sea level of the shuttle. C is a constant that characterizes the lidar system.

[62] $S(z)$ is corrected from the background sky radiance which is simultaneously measured with the lidar profile. *Klett* [1985] gives the solution to the inverse problem:

$$\beta(z) = \frac{S(z) \cdot Q(z)}{\frac{S_0}{\beta_0} + 2/\cos(\theta) \int_z^{z_0} \frac{1}{BER(z)} S(z') \cdot Q(z') \cdot dz'} \tag{A2}$$

where S_0 and β_0 are respectively the signal and the backscatter coefficient at the reference altitude z_0. $Q(z)$ is the correction related to the differential molecular optical thickness calculated from the vertical profile of the molecular scattering coefficient $\alpha_m(z)$:

$$Q(z) = \exp\left(2/\cos(\theta) \cdot \int_z^{z_0} \left[\frac{3}{8\pi \cdot BER(z)} - 1 \right] \cdot \alpha_m(z') \cdot dz' \right) \tag{A3}$$

The molecular contribution is derived from an ancillary climatic database as in the work by *Chazette et al.* [1995]. The aerosol extinction coefficient α_e, which is the sum of the scattering and absorbing coefficients, can then be obtained by

$$\alpha_e(z) = \frac{1}{BER(z)} \left[\beta(z) - 3/8\pi \alpha_m(z) \right] \tag{A4}$$

[63] The lidar-derived aerosol optical thickness (AOT) is calculated as the integral of the extinction coefficient from the ground surface up to the reference altitude z_0:

$$AOT = \int_{ground}^{z_0} \alpha_e(z) dz \tag{A5}$$

[64] Following *Platt* [1981], the *BER*, product of the single scattering albedo and normalized backscatter phase function of aerosols, is given against the apparent BER (*ABER*) by

$$BER(z) = \eta(z) \cdot ABER(z) \tag{A6}$$

[65] The multiple scattering factor η at different depth in the aerosols layer is deduced from the ratio between the total lidar signal S (including single and multiple scattering S_{mul}) and the number of single-backscattered photon as:

$$\eta(z) = 1 - \frac{\ln\left(\frac{S(z)}{S(z) - S_{mul}(z)} \right)}{2 \cdot (AOT(z=0) - AOT(z))} \tag{A7}$$

[66] **Acknowledgments.** We are grateful to B. Marticorena and B. Laurent for dust emission data. This work was supported by the Programme National de Télédétection Spatiale from the Institut National des Sciences de l'Univers (INSU), by the Centre National d'Etudes Spatiales in the frame of the CALIPSO program and by the Commissariat à l'Energie Atomique. The support of Alcatel Space for S. Berthier is greatly acknowledged.

References

Ackerman, S. A., and H. Chung (1992), Radiative effects of airborne dust on regional energy budgets at the top of the atmosphere, *J. Appl. Meteorol.*, *31*, 223–233.

Alpert, P., Y. J. Kaufman, Y. Shay-El, D. Tanré, A. da Silva, S. Schubert, and J. H. Joseph (1998), Quantification of dust-forced heating of the lower troposphere, *Nature*, *395*, 367–370.

Andreae, M. O. (1996), Raising dust in the greenhouse, *Nature*, *380*, 389–390.

Ansmann, A., D. Althausen, U. Wandinger, K. Franke, D. Müller, F. Wagner, and J. Heintzenberg (2000), Vertical profiling of the Indian aerosol plume with six-wavelength lidar during INDOEX: A first case study, *Geophys. Res. Lett.*, *27*(7), 963–966.

Ansmann, A., et al. (2003), Long-range transport of Saharan dust to northern Europe: The 11–16 October 2001 outbreak observed with EARLINET, *J. Geophys. Res.*, *108*(D24), 4783, doi:10.1029/2003JD003757.

Barnaba, F., and G. P. Gobbi (2001), Lidar estimation of tropospheric aerosol extinction, surface area and volume: Maritime and desert-dust cases, *J. Geophys. Res.*, *106*, 3005–3018.

Bergametti, G., L. Gomes, E. Remoudaki, M. Desbois, D. Martin, and P. Buat-Ménard (1989), Present transport and deposition patterns of African dusts to the north-western Mediterranean, in *Paleoclimatology and Paleometeorology: Modern and Past Patterns of Global Atmospheric Transport*, edited by M. Leinen and M. Sarnthein, pp. 227–251, Springer, New York.

Boucher, O. (1995), GCM estimate of the indirect aerosol forcing using satellite-retrieved cloud effective droplet radii, *J. Clim.*, *8*, 1403–1409.

Briegleb, B. P., P. Minnis, V. Ramanathan, and E. Harrison (1986), Comparison of regional clear-sky albedos inferred from satellite observations and model computations, *J. Clim. Appl. Meteorol.*, *25*, 214–226.

Brooks, N., and M. Legrand (2000), Dust variability over northern Africa and rainfall in the Sahel, in *Linking Climate Change to Land Surface Change*, edited by S. J. McLaren and D. R. Kniveton, pp. 1–25, Springer, New York.

Carlson, T. N., and J. M. Prospero (1972), The large-scale movement of Saharian air outbreaks over the northern equatorial Atlantic, *J. Appl. Meteorol.*, *11*, 283–297.

Cattrall, C., J. Reagan, K. Thome, and O. Dubovik (2005), Variability of aerosol and spectral lidar and backscatter and extinction ratios of key aerosol types derived from selected Aerosol Robotic Network locations, *J. Geophys. Res.*, *110*, D10S11, doi:10.1029/2004JD005124.

Cautenet, G., M. Legrand, S. Cautenet, B. Bonnel, and G. Brogniez (1992), Thermal impact of Saharan dust over land, Part I: Simulation, *J. Appl. Meteorol.*, *31*, 166–180.

Charlson, R. J., S. E. Schwartz, J. M. Hales, J. A. Coakley, J. E. Hansen, and D. J. Hofman (1992), Climate forcing by anthropogenic aerosols, *Science*, *255*, 423–430.

Charlson, R. J., T. L. Anderson, and H. Rodhe (1999), Direct climate forcing by anthropogenic aerosols: Quantifying the link between atmospheric sulfate and radiation, *Contrib. Atmos. Phys.*, *72*, 74–79.

Chazette, P. (2003), The monsoon aerosol extinction properties at Goa during INDOEX as measured with lidar, *J. Geophys. Res.*, *108*(D6), 4187, doi:10.1029/2002JD002074.

Chazette, P., C. David, J. Lefrère, S. Godin, J. Pelon, and G. Mégie (1995), Comparative lidar study of the optical, geometrical, and dynamical properties of stratospheric post-volcanic aerosols, following the eruptions of El Chichon and Mount Pinatubo, *J. Geophys. Res.*, *100*(D11), 23,195–23,208.

Chazette, P., J. Pelon, C. Moulin, F. Dulac, I. Carrasco, W. Guelle, P. Bousquet, and P. H. Flamant (2001), Airborne lidar and Meteosat synergy to characterize a Saharan dust plume over the Azores during SOFIA/ASTEX, *Atmos. Environ.*, *35*, 4297–4304.

Chazette, P., J. Pelon, and G. Mégie (2002), Determination of structural parameters of atmospheric scattering layer using spaceborne backscatter lidar, *Appl. Opt.*, *40*, 3428–3440.

Chazette, P., H. Randriamiarisoa, J. Sanak, P. Couvert, and C. Flamant (2005), Optical properties of urban aerosol from airborne and ground-based in situ measurements performed during the ESQUIF program, *J. Geophys. Res.*, *110*, D02206, doi:10.1029/2004JD004810.

Chester, R. (1986), The marine mineral aerosol, in *The Role of Air-Sea Exchange in Geochemical Cycling*, *NATO ASI Ser., Ser. C*, vol. 185, edited by P. Buat-Ménard, pp. 443–471, Springer, New York.

Chiapello, I., and C. Moulin (2002), TOMS and METEOSAT satellite records of the variability of Saharan dust transport over the Atlantic during the last two decades (1979–1997), *Geophys. Res. Lett.*, *29*(8), 1176, doi:10.1029/2001GL013767.

Chu, D. A., Y. J. Kaufman, C. Ichoku, L. A. Remer, D. Tanre, and B. N. Holben (2002), Validation of MODIS aerosol optical depth retrieval over land, *Geophys. Res. Lett.*, *29*(12), 8007, doi:10.1029/2001GL013205.

Couch, R. H., et al. (1991), Lidar In-Space Technology Experiment (LITE): NASA's first in-space lidar system for atmospheric research, *Opt. Eng.*, *30*, 88–95.

Deschamps, P.-Y., F.-M Breon, M. Leroy, A. Podaire, A. Bricaud, J.-C. Buriez, and G. Seze (1994), The POLDER mission: Instrument characteristics and scientific objectives, *IEEE Trans. Geosci. Remote Sens.*, *32*, 598–615.

Deuzé, J. L., M. Herman, P. Goloub, D. Tanré, and A. Marchand (1999), Characterization of aerosols over ocean from POLDER-ADEOS-1, *Geophys. Res. Lett.*, *26*, 1421–1425.

Dickerson, R. R., S. Kondragunta, G. Stenchikov, K. L. Civerolo, B. G. Doddridge, and B. N. Holben (1997), The impact of aerosols on solar ultraviolet radiation and photochemical smog, *Science*, *278*, 827–830.

Di Iorio, T., A. di Sarra, W. Junkermann, M. Cacciani, G. Fiocco, and D. Fuà (2003), Tropospheric aerosols in the Mediterranean: 1. Microphysical and optical properties, *J. Geophys. Res.*, *108*(D10), 4316, doi:10.1029/2002JD002815.

Dulac, F., and P. Chazette (2003), Airborne study of a multi-layer aerosol structure in the eastern Mediterranean observed with the airborne polarized lidar ALEX during a STAAARTE campaign (7 June 1997), *Atmos. Chem. Phys.*, *3*, 1817–1831.

Dulac, F., P. Buat-Ménard, D. Sutton, D. Tanré, G. Bergametti, and M. Debois (1992), Assessment of the African airborne dust mass over the western Mediterranean Sea using meteosat data, *J. Geophys. Res.*, *97*(D2), 2489–2506.

Eloranta, E. W. (1972), Calculation of doubly scattered lidar returns, Ph.D. dissertation, Univ. of Wis., Madison.

Eloranta, E. W. (2002), Lidar multiple scattering models for use in cirrus clouds, paper presented at 21st International Laser Radar Conference, Opt. Soc. of Am., Quebec City, Que., Canada, 8 –12 July .

Flamant, C., V. Trouillet, P. Chazette, and J. Pelon (1998), Wind speed dependence of the atmospheric boundary layer optical properties and ocean surface reflectance as observed by airborne backscatter lidar, *J. Geophys. Res.*, *103*, 25,137–25,158.

Fouquart, Y., et al. (1986), Observations of Saharan aerosols: results of ECLATS field experiment. II: Broadband radiative characteristics of the aerosols and vertical radiative flux divergence, *J. Clim. Appl. Meteorol.*, *25*, 28–37.

Gillette, D. A. (1979), Environmental factors affecting dust emission by wind erosion, in *Saharan Dust*, edited by C. Morales, *SCOPE Rep., 14*, pp. 71–91, John Wiley, Hoboken, N. J.

Ginoux, P., and O. Torres (2003), Empirical TOMS index for dust aerosol: Applications to model validation and source characterization, *J. Geophys. Res.*, *108*(D17), 4534, doi:10.1029/2003JD003470.

Grant, W. B., E. V. Browell, C. F. Butler, and G. D. Nowicki (1997), LITE measurements of biomass burning aerosols and comparisons with correlative airborne lidar measurements of multiple scattering in the planetary boundary layer, in *Advances in Atmospheric Remote Sensing with Lidar*, edited by A. Ansman et al., pp. 153–156, Springer, New York.

Guieu, C., M.-D. Loÿe-Pilot, C. Ridame, and C. Thomas (2002), Chemical characterization of the Saharan dust end-member: Some biogeochemical implications for the western Mediterranean Sea, *J. Geophys. Res.*, *107*(D15), 4258, doi:10.1029/2001JD000582.

Hamonou, E., P. Chazette, D. Balis, F. Dulac, X. Schneider, E. Galani, G. Ancellet, and A. Papayannis (1999), Characterization of the vertical structure of Saharan dust export to the Mediterranean basin, *J. Geophys. Res.*, *104*, 22,257–22,270.

Haywood, J. M., P. Francis, S. Osborne, M. Glew, N. Loeb, E. Highwood, D. Tanré, G. Myhre, P. Formenti, and E. Hirst (2003), Radiative properties and direct radiative effect of Saharan dust measured by the C-130 aircraft during Saharan Dust Experiment (SHADE): 1. Solar spectrum, *J. Geophys. Res.*, *108*(D18), 8577, doi:10.1029/2002JD002687.

Herman, J. R., P. K. Bhartia, O. Torres, C. Hsu, C. Seftor, and E. Celarier (1997), Global distributions of UV-absorbing aerosols from Nimbus 7/TOMS data, *J. Geophys. Res.*, *102*, 16,911–16,923.

Husar, R. B., J. M. Prospero, and L. L. Stowe (1997), Characterization of tropospheric aerosols over the oceans with the NOAA advanced very high resolution radiometer optical thickness operationnal product, *J. Geophys. Res.*, *102*, 16,889–16,909.

Intergovernmental Panel on Climate Change (2001), *Climate Change 2001: The Science of Climate Change—Technical Summary of the Working Group I Report*, World Meteorol. Organ., Geneva, Switzerland.

Jankoviak, I., and D. Tanré (1992), Satellite climatology of Saharan dust outbreaks: Method and preliminary results, *J. Clim.*, *15*, 646–656.
Karyampudi, V. M., et al. (1999), Validation of the Saharan Dust Plume Conceptual Model Using Lidar, Meteosat, and ECMWF Data, *Bull. Am. Meteorol. Soc.*, *80*, 1045–1075.
Kaufman, Y. J., D. Tanré, L. A. Remer, E. F. Vermote, A. Chu, and B. N. Holben (1997), Operational remote sensing of tropospheric aerosol over land from EOS moderate resolution imaging spectroradiometer, *J. Geophys. Res.*, *102*, 17,051–17,067.
Kaufman, Y. J., D. Tanré, J.-F. Léon, and J. Pelon (2003), Retrieval of profiles of fine and coarse aerosols using Lidar and radiometric space measurements, *IEEE Trans. Geosci. Remote Sens.*, *41*(8), 1743–1754.
Key, J. (2001), Streamer user's guide, 96 pp., Coop. Inst. for Meteorol. Satell. Stud., Univ. of Wis., Madison.
Key, J., and A. J. Schweiger (1998), Tools for atmospheric radiative transfer: Streamer and FluxNet, *Comput. Geosci.*, *24*(5), 443–451.
Klett, J. D. (1981), Stable analytical inversion solution for processing lidar return, *Appl. Opt.*, *20*, 211–220.
Klett, J. D. (1985), Lidar inversion with variable backscatter/extinction ratios, *Appl. Opt.*, *24*, 1638–1643.
Laurent, B. (2005), Simulations des émissions d'aérosols désertiques à l'échelle continentale: Analyse climatologique des émissions du nord-est de l'Asie et du nord de l'Afrique, Ph.D. dissertation, Univ. Paris 12, Paris.
Laurent, B., B. Marticorena, G. Bergametti, P. Chazette, F. Maignan, and C. Schmechtig (2005), Simulation of the mineral dust emission frequencies from desert areas of China and Mongolia using an aerodynamic roughness length map derived from the POLDER/ADEOS 1 surface products, *J. Geophys. Res.*, *110*, D18S04, doi:10.1029/2004JD005013.
Legrand, M., G. Cautenet, and J. C. Buriez (1992), Thermal impact of Saharan dust over land. Part II: Application to satellite IR remote sensing, *J. Appl. Meteorol.*, *31*, 181–193.
Legrand, M., C. N'Doumé, and I. Jankowiak (1994), Satellite-derived climatology of the Saharan aerosol, in *Passive Infrared Remote Sensing of Clouds and the Atmosphere II*, edited by D. K. Lynch, *Proc. SPIE Int. Soc. Opt. Eng.*, *2309*, 127–135.
Legrand, M., A. Plana-Fattori, and C. N'Doumé (2001), Satellite detection of dust using the IR imagery of Meteosat: 1. Infrared difference dust index, *J. Geophys. Res.*, *106*, 18,251–18,274.
Léon, J.-F., P. Chazette, J. Pelon, F. Dulac, and H. Randriamiarisoa (2002), Aerosol direct radiative impact over the INDOEX area based on passive and active remote sensing, *J. Geophys. Res.*, *107*(D19), 8006, doi:10.1029/2000JD000116.
Léon, J., D. Tanré, J. Pelon, Y. J. Kaufman, J. M. Haywood, and B. Chatenet (2003), Profiling of a Saharan dust outbreak based on a synergy between active and passive remote sensing, *J. Geophys. Res.*, *108*(D18), 8575, doi:10.1029/2002JD002774.
Liu, W., R. T. Field, R. G. Gantt, and V. Klemas (1987), Measurement of the surface emissivity of turbid water, *Remote Sens. Environ.*, *21*, 97–109.
Liu, Z., N. Sugimoto, and T. Murayama (2002), Extinction-to-backscatter ratio of Asian dust observed with high-spectral-resolution lidar and Raman lidar, *Appl. Opt.*, *41*, 2760–2767.
Marticorena, B., and G. Bergametti (1995), Modeling the atmospheric dust cycle: 1. Design of a soil derived dust production scheme, *J. Geophys. Res.*, *100*, 16,415–16,430.
Marticorena, B., and G. Bergametti (1996), Two-year simulations of the seasonal and interannual changes of the Saharan dust emissions, *Geophys. Res. Lett.*, *23*(15), 1921–1924.
Marticorena, B., G. Bergametti, B. Aumont, Y. Callot, C. N'Doumé, and M. Legrand (1997), Modeling the atmospheric dust cycle: 2. Simulation of Saharan sources, *J. Geophys. Res.*, *102*, 4387–4404.
Marticorena, B., P. Chazette, G. Bergametti, F. Dulac, C. N'Doumé, and M. Legrand (2004), Mapping the aerodynamic roughness length of desert surfaces from the POLDER/ADEOS bi-directional reflectance product, *Int. J. Remote Sens.*, *25*, 603–626.
Mattis, I., A. Ansmann, D. Müller, U. Wandinger, and D. Althausen (2002), Dual-wavelength Raman lidar observations of the extinction-to-backscatter ratio of Saharan dust, *Geophys. Res. Lett.*, *29*(9), 1306, doi:10.1029/2002GL014721.
McCormick, M. P., et al. (1993), Scientific investigations planned for the Lidar In-Space Technology Experiment (LITE), *Bull. Am. Meteorol. Soc.*, *74*, 205–214.
Measures, R. M. (1984), *Laser Remote Sensing*, Wiley-Interscience, Hoboken, N. J.
Moulin, C., and X. Schneider (1999), Calibration of the Meteosat-5 sensor visible channel, *Int. J. Remote Sens.*, *20*, 195–200.
Moulin, C., F. Guillard, F. Dulac, and C. E. Lambert (1997a), Long-term daily monitoring of Saharan dust load over ocean using ISCCP-B2 data: 1. Methodology and preliminary results for 1983–1994 in the Mediterranean, *J. Geophys. Res.*, *102*, 16,947–16,958.
Moulin, C., F. Dulac, C. E. Lambert, P. Chazette, I. Jankowiak, B. Chatenet, and F. Lavenu (1997b), Long-term daily monitoring of Saharan dust load over ocean using ISCCP-B2 data: 2. Accuracy of the method and validation using Sun photometer measurements, *J. Geophys. Res.*, *102*, 16,959–16,969.
Moulin, C., et al. (1998), Satellite climatology of African dust transport in the Mediterranean atmosphere, *J. Geophys. Res.*, *103*, 13,137–13,144.
Murayama, T., et al. (2003), An intercomparison of lidar-derived aerosol optical properties with airborne measurements near Tokyo during ACE-Asia, *J. Geophys. Res.*, *108*(D23), 8651, doi:10.1029/2002JD003259.
Nicolas, F., L. R. Bissonnette, and P. Flamant (1997), Lidar effective multiple scattering coefficients in cirrus clouds, *Appl. Opt.*, *36*, 3458–3468.
Ogawa, K., and T. Schmugge (2004), Mapping surface broadband emissivity of the sahara desert using ASTER and MODIS data, *Earth Interact.*, *8*(7), 1–14.
Pelon, J., C. Flamant, P. Chazette, J. F. Léon, D. Tanré, M. Sicard, and S. K. Satheesh (2002), Characterization of aerosol spatial distribution and optical properties over the Indian Ocean from airborne lidar and radiometry during INDOEX'99, *J. Geophys. Res.*, *107*(D19), 8029, doi:10.1029/2001JD000402.
Pierangelo, C., A. Chédin, S. Heilliette, N. Jacquinet-Husson, and R. Armante (2004), Dust altitude and infrared optical depth from AIRS, *Atmos. Chem. Phys.*, *4*, 1813–1822.
Platt, C. M. R. (1973), Lidar and radiometric observation of cirrus clouds, *J. Atmos. Sci.*, *30*, 1191–1204.
Platt, C. M. R. (1981), Remote sensing of high clouds III. Monte Carlo calculations of multiply scattered lidar returns, *J. Atmos. Sci.*, *38*, 156–167.
Platt, C. M. R., D. M. Winker, M. A. Vaughan, and S. D. Miller (1999), Backscatter-to-extinction ratios in the top layers of tropical mesoscale convective systems and in isolated cirrus from LITE observations, *J. Appl. Meteorol.*, *38*, 1330–1345.
Powell, D. M., J. A. Reagan, M. A. Rubio, W. H. Erxleben, and J. D. Spinhirne (2000), ACE 2 multiple angle micro-pulse lidar observations from Las Galletas, Tenerife, Canary Islands, *Tellus, Ser. B*, *52*, 652–661.
Prospero, J. M., P. Ginoux, O. Torres, and S. E. Nicholson (2002), Environmental characterization of global sources of atmospheric soil dust identified with the Nimbus 7 Total Ozone Mapping Spectrometer (TOMS) absorbing aerosol product, *Rev. Geophys.*, *40*(3), 1002, doi:10.1029/2000RG000095.
Quijano, A. L., I. N. Sokolik, and O. B. Toon (2000), Radiative heating rates and direct radiative forcing by mineral dust in cloudy atmospheric conditions, *J. Geophys. Res.*, *105*(D10), 12,207–12,220.
Randriamiarisoa, H., P. Chazette, and G. Mégie (2004), The columnar retrieved single scattering albedo from NO_2 photolysis rate, *Tellus, Ser. B*, *56*, 118–127.
Remer, L. A., et al. (2001), Validation of MODIS aerosol retrieval over ocean, *Geophys. Res. Lett.*, *29*(12), 1–4.
Rosenfeld, D. (2000), Suppression of rain and snow by urban and industrial air pollution, *Science*, *287*, 1793–1796.
Seinfeld, J. H., and S. N. Pandis (Eds.) (1998), *From Air Pollution to Climate Change: Atmospheric Chemistry and Physics*, 1326 pp., John Wiley, Hoboken, N. J.
Sicard, M., P. Chazette, J. Pelon, J. G. Won, and S. C. Yoon (2002), Variational method for the retrieval of the optical thickness and the backscatter coefficient from multiangular lidar profiles, *App. Opt.*, *41*, 493–502.
Sicard, M., F. Rocadenbosch, M. A. Lopez, A. Comeron, A. Rodriguez, C. Munoz, and D. Garcia-Vizcaino (2003), Characterization of aerosol backscatter-to-extinction ratio from multiwavelength and multi-angular lidar profiles, in *Remote Sensing of Clouds and the Atmosphere VII*, edited by K. P. Schaefer et al., *Proc. SPIE Int. Soc. Opt. Eng.*, *4882*, 442–450.
Spinhirne, J. D. (1982), Lidar clear atmosphere multiple scattering dependence on receiver range, *Appl. Opt.*, *21*, 2467–2468.
Stephens, G. L., R. J. Engelen, M. Vaughan, and T. L. Anderson (2001), Toward retrieving properties of the tenuous atmosphere using space-based lidar measurements, *J. Geophys. Res.*, *106*, 28,143–28,157.
Stowe, L. L., R. M. Carey, and P. P. Pellegrino (1992), Monitoring the Mt. Pinatubo aerosol layer with NOAA/AVHRR data, *Remote Sens. Envron.*, *60*, 22–34.
Stowe, L., A. Ignatov, and R. Singh (1997), Development, validation, and potential enhancements to the second-generation operational aerosol product at the National Environmental Satellite, Data and Information Service of the National Oceanic and Atmospheric Administration, *J. Geophys. Res.*, *102*, 16,923–16,934.
Takemi, T., M. Yasui, J. Zhou, and L. Liu (2006), Role of boundary layer and cumulus convection on dust emission and transport over a

midlatitude desert area, *J. Geophys. Res.*, *111*, D11203, doi:10.1029/2005JD006666.

Tanré, D., C. Deroo, P. Duhaut, M. Herman, J. J. Morchrette, J. Perbos, and P. Y. Deschamps (1986), Simulation of the Satellite Signal in the Solar Spectrum (5S), users's guide, Lab. d'Opt. Atmos., Univ. des Sci. et Technol. de Lille, Villeneuve d'Ascq, France.

Tanré, D., Y. Kaufman, M. Herman, and S. Mattoo (1997), Remote sensing of aerosol properties over the oceans using the MODIS/EOS spectral radiances, *J. Geophys. Res.*, *102*, 16,971–16,988.

Volz, F. E. (1973), Infrared optical constants of ammonium sulfate, Saharan dust, volcanic pumice and fly-ash, *J. Appl. Opt.*, *12*, 564–568.

Welton, E. J., et al. (2000), Ground-based lidar measurements of aerosols during ACE-2: Lidar description, results, and comparisons with other ground-based and airborne measurements, *Tellus, Ser. B*, *52*, 636–665.

Wiegner, M., U. Oppel, H. Krasting, W. Renger, C. Kiemle, and M. Wirth (1996), Cirrus measurements from a spaceborne lidar: Influence of multiple scattering, in *Advances in Atmospheric Remote Sensing With Lidar*, edited by A. Ansmann et al., pp. 189–192, Springer, New York.

Winker, D. M., M. P. McCormick, and R. Couch (1996), An overview of LITE: NASA's Lidar In-space Technology Eperiment, *Proc. IEEE*, *84*, 164–180.

Winker, D. M., J. Pelon, and M. P. McCormick (2002), The CALIPSO mission: Spaceborne lidar for observation of aerosols and clouds, *Proc. SPIE Int. Soc. Opt. Eng.*, *4893*, 1–11.

Yasui, M., J. Zhou, L. Liu, T. Itabe, K. Mizutani, and T. Aoki (2005), Vertical profiles of aeolian dust in the desert atmosphere observed by a lidar in Shapotou China, *J. Meteorol. Soc. Jpn.*, *83A*, 149–171.

Zwally, H. J., et al. (2002), ICESat's laser measurements of polar ice, atmosphere, ocean, and land, *J. Geodyn.*, *34*, 405–445.

S. Berthier and J. Pelon, Service d'Aéronomie, CNRS, Université Paris VI Tour 45, Aile 45/46, 3^{e} et 4^{e} étage, Boite 102, 4, place Jussieu, F-75252 Paris Cedex 05, France. (sebastien.berthier@cea.fr)

P. Chazette, F. Dulac, C. Moulin, and F. Thieuleux, LSCE-Orme, Bât. 701, Orme des Merisiers, F-91191 Gif-Sur-Yvette Cedex, France.

T. Pain, Alcatel Space, Bp 99, 100 Bld Du Midi, F-06156 Cannes la Bocca, France.